ACS Photonics

pubs.acs.org/journal/apchd5

Review

The Path to Enlightenment: Progress and Opportunities in High Efficiency Halide Perovskite Light-Emitting Devices

Chen Zou, Congyang Zhang, Young-Hoon Kim, Lih Y. Lin,* and Joseph M. Luther*

Cite This: ACS Photonics 2021, 8, 386−404

Read Online

ACCESS | Metrics & More | Article Recommendations

ABSTRACT: Besides the flourishment in photovoltaics, halide perovskites hold great promise to compete with leading contenders among solution-processed emitters, such as organics and semiconductor colloidal nanocrystals, in the field of light emission. Halide perovskites exhibit outstanding optoelectronic properties, including high photoluminescence quantum yields, facile bandgap tunability, narrow emission line widths, and respectable carrier mobilities, promoting them to thrive in versatile light-emitting applications such as light-emitting diodes, lasers, X-ray scintillators, and circularly polarized light sources. Herein, we discuss the underlying physics of light emission in state-of-the-art perovskite light-emitting devices and focus on promising strategies for further improvement of device performance.

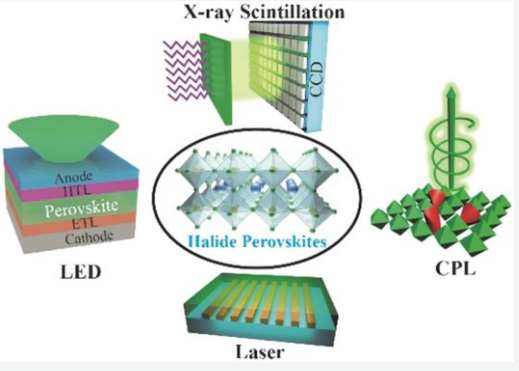

KEYWORDS: halide perovskites, light-emitting diodes, lasers, X-ray scintillators, circularly polarized luminescence, device physics

Halide perovskites slowly emerged into the spotlight for photovoltaic applications starting in 2009, but not really attracting attention until 2013. Since then, perovskite solar cells have undergone rapid development with the highest reported power conversion efficiency (PCE), increasing from 3.8% to over 25% in single-junction architectures, now comparable to the state-of-the-art Si solar cells.[1,2] Generally, halide perovskites can be represented by an ABX_3 composition, where A is a large monovalent cation (methylammonium $CH_3NH_3^+$ (MA^+) or formamidinium $CH(NH_2)_2^+$ (FA^+) or cesium Cs^+), B is a divalent metal cation (typically Pb^{2+}, Sn^{2+}, Ge^{2+}, etc.), and X is a halogen anion (Cl^-, Br^-, I^-). Besides great success in the field of photovoltaics, the additional advantages of perovskites, including high photoluminescence quantum yield (PLQY) approaching 100%,[3−6] respectable carrier mobility in excess of 10 $cm^2\ V^{-1}\ s^{-1}$,[7,8] widely tunable emission wavelength and narrow emission line width motivate researchers to explore their applications in the field of light emission. In particular, emission wavelengths of perovskite films can be easily tuned from ultraviolet (UV) to near-infrared (NIR) by changing their composition and dimensionality, leading to a wide color gamut (≈140%) that is broader than the National Television System Committee (NTSC) standard on a CIE chromaticity diagram. Meanwhile, perovskites exhibit narrow and symmetric PL spectra (full width at half-maximum fwhm ≈ 12−40 nm), leading to a high color purity suited for more vivid and natural color displays.[9] Moreover, halide perovskites can have various crystal forms such as single crystals, polycrystalline bulk films, and colloidal nanocrystals, endowing diverse research directions to researchers.[10,11]

After decades of development, organic semiconductors and colloidal metal chalcogenide or pnictide semiconductor nanocrystals (colloidal nanocrystals hereafter) have become leading emitter candidates in the commercial market of flat panel displays. Vivid, high color purity displays could become more mainstream if emitters can be developed with narrower emission spectra than organic emitters (fwhm ∼ 50 nm) and colloidal nanocrystals (fwhm ∼ 20−40 nm). Halide perovskites and related perovskite-inspired materials with controllable dimensionalities have attracted researchers' attention for their bright luminescence with narrow emission spectra (fwhm ∼ 20 nm) and simple fabrication/synthesis, even in ambient conditions at room temperature. The past five years have witnessed an unprecedented advance in the field of light emission in halide perovskites, which may advance more quickly than previous technologies by building on existing achievements from organic light-emitting diodes (OLEDs) and quantum dot LEDs (QLEDs) over the last few decades, just as perovskite photovoltaic (PV) advanced rapidly from existing

Received: September 8, 2020
Published: January 20, 2021

https://dx.doi.org/10.1021/acsphotonics.0c01394
ACS Photonics 2021, 8, 386−404

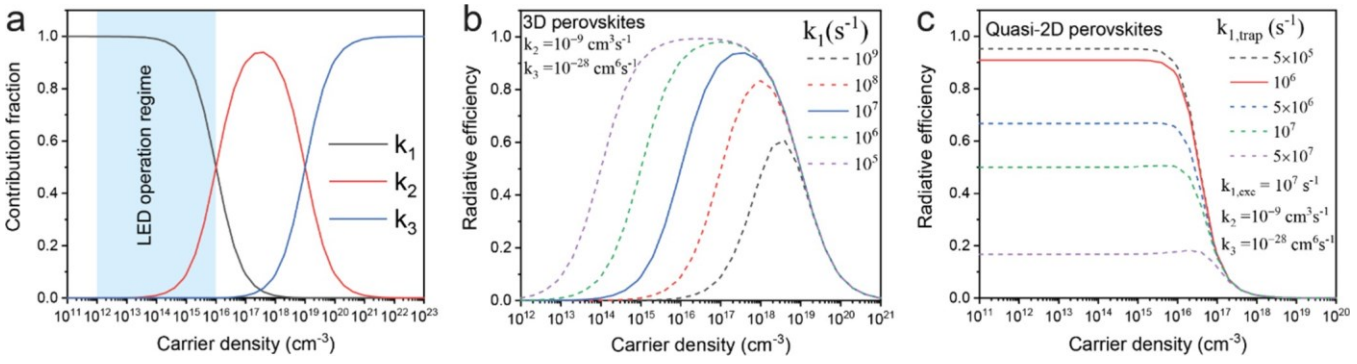

Figure 1. (a) Individual fractions of molecular, bimolecular, and Auger recombination contributing to overall recombination at various carrier densities. Typical values of $k_1 \approx 10^7\ s^{-1}$, $k_2 \approx 10^{-9}\ cm^3\ s^{-1}$, and $k_3 \approx 10^{-28}\ cm^6\ s^{-1}$ for 3D perovskites were taken from literature. (b) Calculated radiative efficiency vs charge-carrier density varying k_1 values for 3D perovskites, while k_2 and k_3 values are fixed. (c) Calculated radiative efficiency vs charge-carrier density for quasi-2D perovskites with different $k_{1,trap}$ values, while $k_{1,exc}$, k_2, and k_3 values are fixed.

knowledge in the fields of dye-sensitized, organic, and QD PVs.[12,13]

Tan et al. developed the first perovskite light-emitting diodes (PeLEDs) at room temperature using 3D polycrystalline films ($MAPbX_3$) in 2014.[14] The maximum external quantum efficiency (EQE) achieved at that time was 0.76%, far inferior to those of OLEDs and QLEDs. Nevertheless, this pioneering work inspired more PeLED research, leading to EQEs of ~20%, which unambiguously proved the prospect of 3D perovskites as next-generation light emitters.[15−17] In a parallel development with 3D perovskites, quasi-2D perovskites were rediscovered and applied successfully in high-efficiency PeLEDs by the Sargent and Huang groups in 2016.[18,19] The quasi-2D perovskites refer to a perovskite family with the chemical formula $L_2A_{n-1}M_nX_{3n+1}$, where L is a larger organic, typically ammonium, cation (e.g., phenylethylammonium (PEA) and butylammonium (BA)). The assembly of layered perovskites forms structures akin to multiple quantum wells (MQWs) and leads to high EQEs of over 20.1% and 11% for NIR and sky-blue emitting PeLEDs, respectively.[6,20] Perovskite nanocrystals (NCs), benefiting from quantum confinement and surface passivation, have shown outstanding performance in PeLEDs as well. Blue, green, and red perovskite NC LEDs have achieved peak EQEs of 12.3%, 22%, and 21.3%, respectively.[21,22] In addition to efficient luminescence, strong coherent emission properties of perovskites contribute to their remarkable performance in lasing applications. It is also encouraging that continuous-wave (CW) amplified spontaneous emission (ASE) and lasing of perovskites have been demonstrated recently.[23−25]

In this Review, we first examine the underlying photophysics of various effective approaches to obtain highly luminescent perovskite films, then we provide a brief review on the progress and opportunities of halide perovskites in the field of light-emission applications, including LEDs, lasers, X-ray scintillators, and circularly polarized light sources. For commercial applications, far more attention needs to be devoted toward understanding and improving the stability of perovskite materials and devices. However, here we focus more on the light-emission properties of perovskites and, therefore, point interested readers to existing literature focused on stability.[26−28]

BRIGHT PEROVSKITE EMITTERS

What Do the Recombination Dynamics Tell Us?

PL emission originates from the radiative recombination of photogenerated charge carriers, in competition with nonradiative recombination processes. The general charge carrier recombination kinetics can be described as below:[29]

$$\frac{dn(t)}{dt} = -k_1 n - k_2 n^2 - k_3 n^3 \quad (1)$$

where t is time and n is charge carrier density. k_1, k_2, and k_3 are monomolecular, bimolecular, and Auger recombination rate constants, respectively. Monomolecular recombination can be divided into trap-assisted Shockley-Read-Hall recombination ($k_{1,trap}$), excitonic recombination ($k_{1,exc}$), and pseudo-first-order recombination ($k_{1,dopant}$) of photogenerated carriers with dopant carriers.[30] The former is nonradiative, while the latter two can be radiative. Bimolecular recombination is a radiative process dominated by free electron−hole pairs. Auger recombination is a three-particle nonradiative process, where the energy released upon recombination of an electron−hole pair excites the third carrier rather than creating a photon.

To obtain a high-PLQY light emitter, the proportion of the radiative recombination to total recombination should be maximized. Assuming typical values of $k_1 \approx 10^7\ s^{-1}$, $k_2 \approx 10^{-9}\ cm^3\ s^{-1}$, and $k_3 \approx 10^{-28}\ cm^6\ s^{-1}$ for 3D perovskites,[8,29,31,32] we show that the dominant recombination pathway changes with increasing carrier density (Figure 1a). At low carrier densities ($n < 10^{15}\ cm^{-3}$), charge carriers mainly undergo monomolecular recombination. In the regime of 10^{15}~$10^{18}\ cm^{-3}$, radiative bimolecular recombination starts to take precedence over other pathways. At high carrier densities ($n > 10^{18}\ cm^{-3}$), many-body Auger recombination dominates.[33] In the LED operation regime ($n = 10^{12}$~$10^{16}\ cm^{-3}$), k_1 may be the most crucial factor affecting the PLQY of 3D perovskites compared with k_2 and k_3.[29] Given the relatively small exciton binding energy (E_b) of 3D perovskites at room temperature,[34,35] their photogenerated excitons can be quickly dissociated into free electrons and holes, leading to a negligible $k_{1,exc}$. In addition, $k_{1,dopant}$ is usually much less than $k_{1,trap}$ in 3D perovskites.[36] Thereby, we can generally assume $k_1 \approx k_{1,trap}$, and the PLQY of 3D perovskites (η_{3D}) can be expressed as[32]

$$\eta_{3D} = \frac{k_2 n}{k_1 + k_2 n + k_3 n^2} \quad (2)$$

https://dx.doi.org/10.1021/acsphotonics.0c01394
ACS Photonics 2021, 8, 386−404

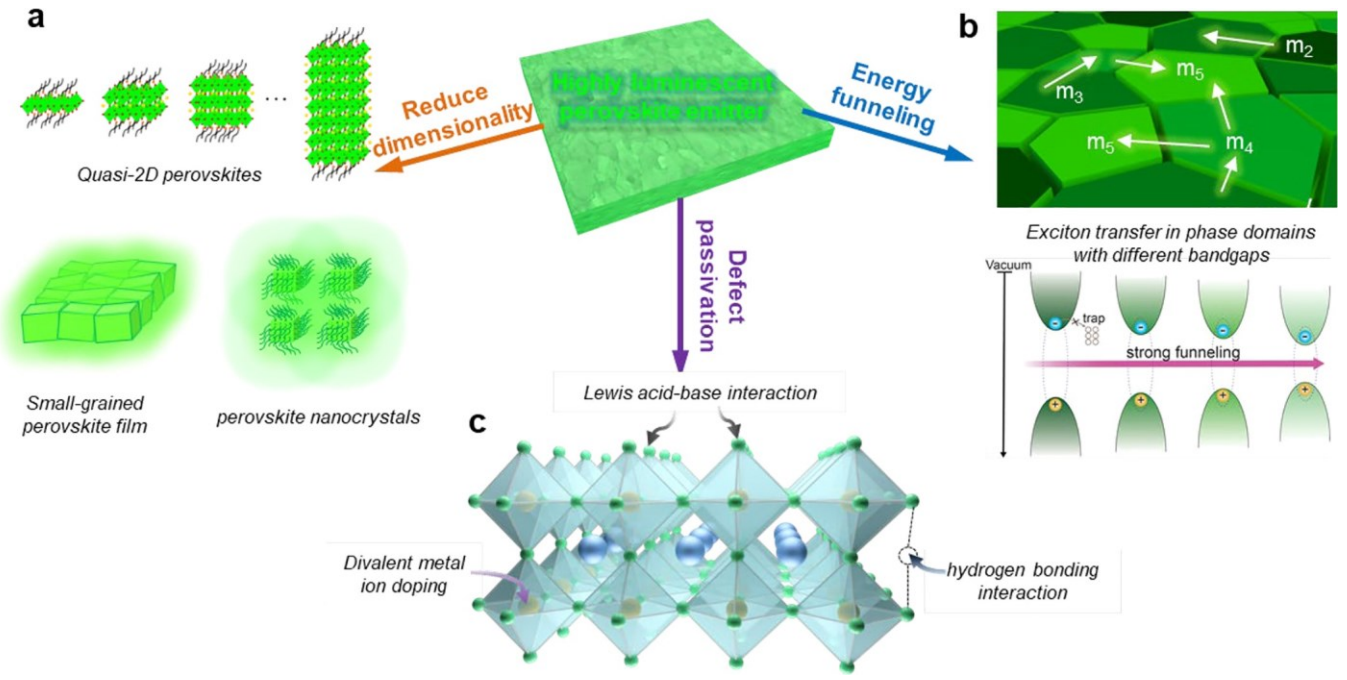

Figure 2. Promising strategies for obtaining highly luminescent perovskite films, including (a) excitonic recombination enhancement, (b) energy funneling modulation, and (c) defect passivation.

Since radiative processes of 3D perovskites are dominated by free-carrier bimolecular recombination, the η_{3D} value would not rise with increasing carrier density until $k_2 n$ starts to outrank k_1. Therefore, it is understandable why early developed 3D PeLEDs (with high k_1 values) show relatively poor performance. η_{3D} peaks at a carrier density of $n = \sqrt{k_1/k_3}$ with a maximum value of $\eta_{max} = \frac{1}{1 + 2(k_1 k_3)^{0.5}/k_2}$. The reduction of the k_1 value can not only increase η_{3D}, but also shifts the η_{3D} peak toward the low carrier-density regime, which is beneficial to PeLED operation (Figure 1b). Meanwhile, it is also nontrivial to increase k_2, as this will bring about a broadening of the PLQY peak that will extend into both the low and high carrier density regions, which could further improve the peak EQE of PeLEDs and suppress the efficiency roll-off.

In the case of quasi-2D perovskites and perovskite NCs, strong quantum confinement leads to enhanced E_b, changing the leading dynamics in monomolecular recombination from nonradiative trap-assisted to radiative excitonic recombination. At the same time, this also shifts dominant radiative processes from second-order bimolecular to first order excitonic recombination which peaks at a lower carrier density. The PLQY of quasi-2D perovskites and perovskite NCs ($\eta_{0D/2D}$) can be described by[37]

$$\eta_{0D/2D} = \frac{k_{1,exc} + k_2 n}{k_{1,exc} + k_{1,trap} + k_2 n + k_3 n^2} \quad (3)$$

where the monomolecular recombination rate (k_1) is split into an exciton radiative rate ($k_{1,exc}$) and a trap-assisted nonradiative rate ($k_{1,trap}$). We calculated the dependence of $\eta_{0D/2D}$ on carrier density using different $k_{1,trap}$ values (Figure 1c). It is noticeable that there is a regime with nearly invariant PLQY at low carrier densities. The near-constant PLQY value is determined by $k_{1,exc}/(k_{1,exc} + k_{1,trap})$. When $k_{1,exc}$ is much greater than $k_{1,trap}$, high PLQY values can be obtained for a wide range of carrier densities in the LED operation regime. Therefore, both enhancing excitonic recombination via E_b modulation and reducing defect state densities should be considered for quasi-2D perovskites and perovskite NCs.

Strategies to Boost PLQY. Based on the analysis from the view of photophysics, we have concluded three generic strategies that can be effective to boost the PLQY of perovskite emitters (Figure 2).

Enhance Excitonic Recombination. Enhancing the E_b is a key strategy to improve the excitonic recombination rate in perovskites (Figure 2a). In 3D perovskites, reducing grain size is an effective way to provide some degree of quantum confinement and thus increase E_b. Solvent nanocrystal pinning (S-NCP) can facilitate the uniform growth of small grains in perovskite films.[38] In addition, ligands or additives in perovskite precursors can control crystal growth kinetics, benefiting the high-PLQY perovskite film with reduced grain size and enhanced E_b.[39,40]

From the perspective of quantum confinement promoting radiative excitonic recombination, it is not strange to see that perovskite NCs have shown superior PLQYs intrinsically. In contrast with the relatively small E_b (65 meV) of bulk $MAPbBr_3$, $MAPbBr_3$ NCs exhibited a remarkably larger E_b (up to 375 meV).[41] As a consequence, the PLQY of the colloidal solution reached over 70%.[41,42] Similarly, quasi-2D perovskites can provide strong quantum confinement originating from MQWs.[18,19,43,44] A high PLQY up to 60% was already achieved when they were first rediscovered in 2016.[19]

Energy Funneling. Although quasi-2D perovskites possess intrinsic radiative excitonic recombination, it is still essential to build up an efficient energy funneling channel to avoid exciton quenching. Solution processed quasi-2D perovskite films usually consist of multiple phase domains with different n values. Such an inhomogeneous energy distribution can funnel energy from larger bandgap phases (lower n) to smaller bandgap phases (higher n) rapidly (within ~50 ps).[29] The ultrafast exciton transfer can essentially outcompete non-

https://dx.doi.org/10.1021/acsphotonics.0c01394
ACS Photonics 2021, 8, 386−404

Table 1. Summary of High-PQLY Perovskite Emitters

emitting materials	improvement strategy	PL wavelength (nm)	PLQY (%)/excitation power (mW/cm^2)	ref
3D (Cs,FA,MA)$Pb(I_{0.85}Br_{0.15})_3$-KI	potassium passivation	~800	~95/~1200	4
3D $CsPbBr_3$-PEO	PEO additive in precursor	521	60	40
3D FAPbI3-DDS	DDS additive in precursor	~800	~85/~65	51
3D $CsPbBr_3$-MABr	MABr passivation	528	~80	15
3D $FAPbI_3$-5-AVA	5-AVA passivation	800	~70/~1−100	17
OPA-$CsPbBr_3$ NCs	OPA ligand passivation	~516	~90[a]	57
DDAB-$CsPbBr_3$ NCs	DDAB ligand passivation	510	80[a]	73
DAT-$CsPb(Br_xCl_{1-x})_3$ NCs	DTA ligand passivation	469	100[a]	3
DBSA-$CsPbBr_3$ NCs	DBSA ligand passivation	~513	>90[a]	59
An-HI-$CsPbI_3$ NCs	An-HI ligand passivation	644	69[a] (21)	21
NH_4SCN-$CsPbBr_3$ NCs	NH_4SCN post-treatment	~510	100[a]	60
KBr-$CsPbI_{3-x}Br_x$ NCs	KBr post-treatment	~640	93[a]	62
$CdCl_2$-$CsPbCl_3$ NCs	$CdCl_2$ post-treatment and doping	406	98[a]	67
$ZnBr_2$-$CsPbBr_3$ NCs	$ZnBr_2$ post-treatment	514	93[a]	61
Ni-$CsPbCl_3$ NCs	Ni^{2+} doping	~406	96.5[a]	69
quasi-2D $(NMA)_2(FA)_{m-1}Pb_mBr_{3m+1}$	precursor stoichiometry modulation	~780	~70/3.5	33
quasi-2D (PEA, IPA)$_2(MA)_{m-1}Pb_mBr_{3m+1}$	using PEA and IPA as co-organic spacer	477	88	74
quasi-2D $(PEA)_2(FAPbBr_3)_{m-1}PbBr_4$-TOPO	TOPO surface passivation	~532	73.8	50
quasi-2D $(PEA)_2Cs_{2.4}MA_{0.6}Pb_4Br_{13}$-TPPO	TPPO surface passivation	517	98/2.3	63
quasi-2D (PEA)$_2$(Rb, Cs)$_{m-1}Pb_mBr_{3m+1}$-RbBr	RbBr passivation	476	82/~1−100	75
quasi-2D $(PEA)_2Cs_{m-1}Pb_mBr_{3m+1}$-crown	crown additive in precursor	~515	70 ± 8/1.5	76

[a]The PLQY value is measured in a colloidal suspension in a solvent; otherwise, the PLQY is measured on a thin-film.

radiative loss caused by defect trapping (Figure 2b). However, the distribution of phase domains needs to be modulated such that energy is funneling from larger bandgap domains into a small subpopulation of narrower bandgap domains.[45] Moreover, the spatial distribution for each of the phase domains should be uniform to prevent energy accumulation in unwanted areas without low bandgap domains. The energy funneling can be regulated through engineering control of the stoichiometry, solvent, composition, and additive. The dimensionality of quasi-2D perovskites can be tuned by varying the amount of the organic spacer, which can subsequently change the pathway of energy funneling. Various organic solvents can be added to control the arrangement of perovskite layers and grains, the high boiling point of toluene would facilitate the unitary distribution of phase domains (flat energy landscape), while chloroform, with faster evaporation, would lead to the graded distribution of domains with different bandgaps and thus higher radiative efficiency.[45] Rational selection and design of organic spacers also affect the distribution of phase domains.[46] Yuan et al. employed a dual organic spacer strategy to modulate the domain distribution, leading to a high-quality perovskite film with deep-blue emission (465 nm) and a PLQY up to 77%. Specifically, the mixed spacer system enabled them to simultaneously suppress n = 1 perovskite domains that have severe recombination pathways and increase the number of n = 3 domains that represents the population of emission species.[47] Besides the regulation of phase domains, Qin et al. found quenching of triplet excitons by the organic cation is a major loss path in quasi-2D perovskite films, which competes with the energy transfer from larger bandgap perovskites to narrower bandgap perovskites. By employing an organic cation with a high triplet energy level (PEA), they achieved a quasi-2D PeLED with a EQE of 12.4%. In contrast, the use of 1-naphthylmethylamine (NMA) with a low triplet energy level leads to a poor performance.[48]

Defect Passivation. In typical 3D perovskites, crystal defects are mainly generated at grain boundaries or on crystal surfaces. These defects act as luminescence quenching centers, accounting for nonradiative recombination loss. To date, many organic molecules and inorganic salts have been employed to passivate defects through Lewis acid−base and hydrogen-bonding interactions (Figure 2c). Specifically, ethylenediamine (EDA), n-trioctylphosphine oxide (TOPO), poly(ethylene oxide) (PEO), 4,4′-diaminodiphenyl sulfone (DDS), LiBr, KBr, and so on can be regarded as Lewis bases to passivate uncoordinated Pb or halide vacancy defects (Lewis acids).[40,49−53] Besides, ammonium-based cations, such as MA^+, fluorophenylmethylammonium ($FPMA^+$), and so on, have been used for passivating defects through hydrogen-bonding interactions with PbX_6^{4-} octahedral. The ammonium cations are routinely employed together with Lewis bases, including halide anions (X^-), trifluoroacetate (TFA^-), carboxyl (−COOH), and so on.[15,17,54,55]

For perovskite NCs, commonly used long-chain organic ligands, such as oleic acid (OA) and oleylamine (OLA), can easily detach from NC surfaces, inducing surface traps, NC aggregation, and poor PL emission. However, colloidal synthesis dictates that the ligands attach to the surface, which may not be the case in thin film crystallization. In NCs, ligand exchange or passivation is of great significance and indispensable for perovskite NC emitters with high PLQYs. Generally, effective passivation agents are organic molecules, inorganic salts, or their hybrids with strong bonding affinity, such as didodecyl dimethylammonium bromide (DDAB),[56] octylphosphonic acid (OPA),[57] 2,2′-iminodibenzoic acid (IDA),[58] n-dodecylammonium thiocyanate (DAT),[3] dodecylbenzenesulfonic acid (DBSA),[59] aniline hydoroiodide (An-HI),[21] ammonium thiocyanate (NH_4SCN),[60] $ZnBr_2$,[61] KBr,[62] and so on. For instance, through a post-treatment with NH_4SCN, the PLQYs of both fresh and aged $CsPbBr_3$ NCs increased to 100% because of strong Lewis acid−base

https://dx.doi.org/10.1021/acsphotonics.0c01394
ACS Photonics 2021, 8, 386−404

interaction between SCN^- and Pb.[60] Defect passivation is nontrivial for quasi-2D perovskites as well since the inhomogeneous domain distribution brings in phase impurity and defects. Through strong Lewis acid−base interaction between P=O and Pb, triphenylphosphine oxide (TPPO) was demonstrated effective to passivate and stabilize the edge state of quasi-2D perovskites $PEA_2Cs_{n-1}Pb_nBr_{3n+1}$ (n = 3), leading to an excellent PLQY of close to 100%.[63]

Apart from surface defects, structure-related defects, typically originated from local lattice strain, short-range lattice disorder, and so on, also have an impact on the PLQY. In this vein, cation doping/incorporation can alleviate or overcome this problem.[64,65] Specifically, in some cases, the A-site cations in corner-shared PbX_6^{4-} octahedral units lead to slight tilting of octahedral units, which can generate trapping centers through affecting the short-range order of lattice.[66] Therefore, metal cation doping (Cd^{2+}, Mn^{2+}, Ni^{2+}, Sr^{2+}, etc.) at B-site or monovalent cation alloying at A-site can suppress this tilting or distortion to some extent, thus, significantly reduce the density of trap states.[67−72] Furthermore, the relaxation of lattice strain can further improve the thermodynamic stability.

Comparison of Various Perovskite Emitters for Light-Emitting Applications. Benefiting from the rapid progress of fabrication techniques for perovskite films in the past several years, all above-mentioned perovskite materials, including 3D, quasi-2D perovskites, and perovskite NCs, are capable of achieving high PLQYs for LED and display applications.[32] We summarize these high-PLQY perovskite emitters in Table 1. For the coherent light emission applications such as lasing, 3D perovskites may have advantages over perovskite NCs because of a reduced contribution from Auger recombination at high carrier densities and more accessibility of intense current injection due to the absence of insulating organic ligand or spacer.[53] For quasi-2D perovskites and NCs, the organic spacers or ligands are indispensable for efficient PL emissions and even the formation of the stacked 2D-layer structure or colloidal dispersion; however, they can hinder the charge injection and transportation in devices as well. Hence, this trade-off between high PLQY and electrical conductivity should be taken into great consideration.

LEDS EXPLOITING PEROVSKITE EMITTERS

Limiting Factors on PeLED Efficiency. A typical PeLED stack is composed of anode, hole transport layer (HTL), perovskite emitter, electron transport layer (ETL) and cathode. The EQE of a PeLED can be described by the following equation:[77]

$$\mathrm{EQE} = \eta_{out}\mathrm{IQE} = \eta_{out}\gamma_{bal}\gamma_{e-h}\eta_{S/T}q_{eff} \quad (4)$$

where η_{out} is the light outcoupling efficiency and IQE is the internal quantum efficiency, which is the product of charge injection balance (γ_{bal}), probability of forming electron−hole pairs (γ_{e-h}), singlet/triplet capture ratio ($\eta_{S/T}$), and effective radiative quantum yield (q_{eff}). Generally, the $\eta_{S/T}$ is close to unity for perovskite films, thus, we can usually neglect this term.[78] By analyzing eq 4, several conditions should be satisfied to achieve a high-efficiency PeLED. (1) Charge injection balance (increase γ_{bal}): the number of electrons and holes should be as similar as possible so that all charge carriers are likely to be paired for radiative recombination. (2) Negligible leakage current (increase γ_{e-h}): the probability of charge carriers passing through the perovskite layer without recombining should be minimized. (3) High PLQY emitters (increase q_{eff}): the nonradiative recombination should be suppressed, especially under LED operation condition where the carrier density is typically less than 10^{16} cm^{-3}. (4) High light outcoupling efficiency (increase η_{out}): the power fraction of outcoupled light from PeLEDs to air should be maximized.

Strategies to Improve EQE. Based on these criteria, we provide promising strategies to improve device efficiency of PeLEDs (Figure 3). Among them, we have illustrated effective

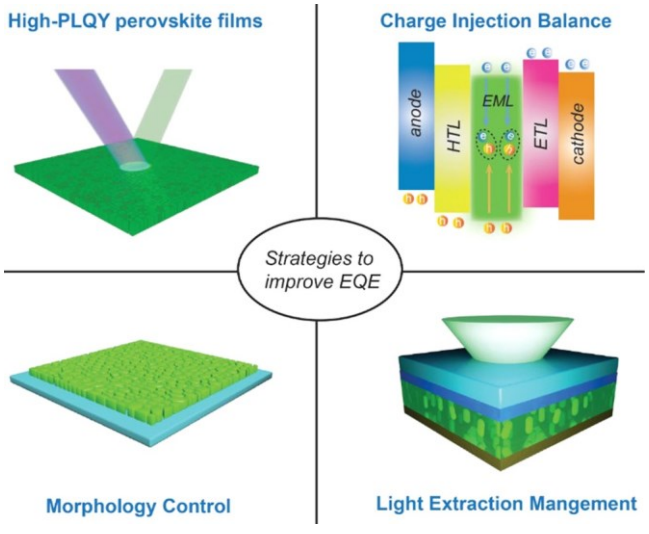

Figure 3. Promising strategies for improving the device efficiency of PeLEDs.

methods to prepare high PLQY perovskite films in Bright Perovskite Emitters. Therefore, we will focus on other strategies in the following.

Charge Injection Balance. Charge injection balance is important in determining the device efficiency of PeLEDs. In addition, unbalanced charge injection favors Auger recombination at high current densities, exacerbating efficiency roll-off (droop) and limiting achievable brightness.[79] Yang et al. found MA- and FA-based quasi-2D perovskites (n = 3 composition) show similar PLQYs; however, the FA-based perovskite exhibits a much higher external quantum efficiency (15.4%) than the MA-based perovskite (0.93%) in LEDs, which could be attributed to the poor hole injection into the MA-based quasi-2D perovskite due to the existing n = 1 phase domains.[80]

To balance electron and hole injection, one can select proper charge transport layers and tune their properties such as thickness and carrier mobility. To slow down electron injection, a thin insulator layer with an optimized thickness can be inserted between the ETL and perovskite layer (Figure 4a).[15,72] In addition, Fakharuddin et al. showed that doping the ETL (4,7-diphenyl-1,10-phenanthroline, bphen) with a small molecule, such as tris(8-hydroxy-quinolinato) aluminum (Alq_3), can decrease the electron mobility (Figure 4b).[81] To facilitate hole injection, Zou et al. adopted a stepwise HTL to reduce hole-injection barrier between the ITO and perovskite layer.[53] Kim et al. designed a high work-function HTL by incorporating perfluorinated ionomer (PFI) into conventional poly(3,4-ethylenedioxythiophene) polystyrenesulfonate (PEDOT:PSS).[82] PeLEDs with modified HTL showed 300-fold improved current efficiency over those with conventional PEDOT:PSS. Engineering perovskite materials has been proven effective as well. Wang et al. reduced the average

https://dx.doi.org/10.1021/acsphotonics.0c01394
ACS Photonics 2021, 8, 386−404

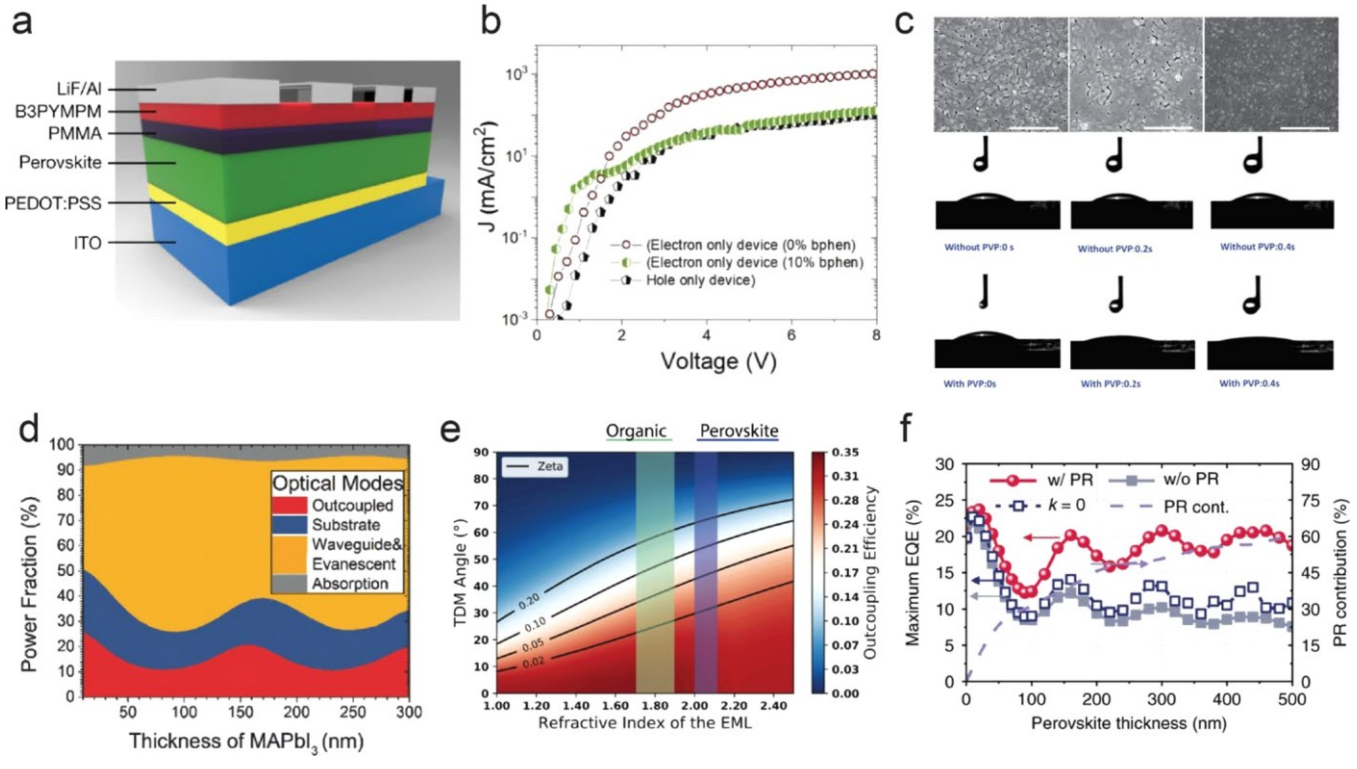

Figure 4. (a) Enhancing PeLED performance by inserting a very thin PMMA layer between the perovskite and the ETL. (b) Current density−voltage curves for electron-only and hole-only devices, the electron-only device with bphen-doped ETL shows reduced current density. (c) Top panel: SEM images (from left to right) of $CsPbBr_3$ deposited on ZnO, ZnO/PVP and $Cs_{0.87}MA_{0.13}PbBr_3$ on ZnO/PVP, respectively. Bottom panel: real time contact angle measurements of perovskite precursor on ZnO and ZnO/PVP. (d) Power distribution in different optical modes of PeLEDs as the thickness of the $MAPbI_3$ layer varies. (e) Dependence of outcoupling efficiency on the angle of the emissive transition dipole moments (TDM) and the refractive index of the emitter. (f) Simulated EQEs with PR (closed red circles), without PR (closed gray squares), and without reabsorption (open navy squares), as well as relative PR contribution (violet dashed lines) for a perfect PeLED (IQE = 100%) with various perovskite layer thickness. (a) Reprinted with permission from ref 15. Copyright 2018 Springer Nature. (b) Reprinted with permission from ref 81. Copyright 2019 John Wiley and Sons. (c) Reprinted with permission from ref 72. Copyright 2017 Springer Nature. (d) Reprinted with permission from ref 78. Copyright 2018 John Wiley and Sons. (e) Reprinted with permission from ref 96. Copyright 2020 Elsevier. (f) Reprinted with permission from ref 95. Copyright 2020 Springer Nature.

interdot distance between perovskite NCs to argument hole mobility for a more balanced charge transport.[83] Zhang et al. fabricated a vertically orientated highly crystalline quasi-2D perovskite film with the assistance of an ammonium thiocyanate (NH_4SCN) additive.[84] The hole mobility increased 100 times to $(2.28 \pm 0.56) \times 10^{-3}$ cm^2 V^{-1} s^{-1}, compared with the randomly oriented film. As a result, more balanced electron and hole transport was achieved with the value of μ_e/μ_h declining from 89.4 to 1.19.

Uniform and Luminescent Perovskite Films. Morphology control also plays a significant role in the performance of PeLEDs. Poor surface morphology accompanied by pinholes would lead to a low-resistance shunting path and nonradiative losses at grain boundaries. Spin-coating is widely used in fabricating solution-processed perovskite films. However, disconnected island-type crystal grains are usually formed in perovskite films, presumably due to growth of perovskite crystals (up to micron-size) and dewetting of perovskite precursor solution on underlying substrates.[85,86]

To fabricate a smooth perovskite film with good coverage, many strategies have been undertaken. An antisolvent-dripping technology (i.e., solvent nanocrystal pinning (S-NCP)) was adopted to induce fast and uniform crystallization, which yields a smooth perovskite film with uniformly small grains.[38,86] A compositional engineering method based on the stoichiometric control of precursor solution was also reported. Zhang et al. showed that a small amount of MABr added into the $CsPbBr_3$ precursor could improve film morphology greatly (Figure 4c).[72] They hypothesized that molecular pinning would better control the crystallization kinetics of the $CsPbBr_3$ films, leading to a perovskite film with a negligible density of pinholes. The quasi-2D Ruddlesden−Popper (RP) structure is another choice to obtain high-quality films. The incorporation of bulky alkylammonium cations like PEABr hinders crystal growth during crystal pinning, forming smooth perovskite films with minimal surface roughness less than 1 nm.[18] Additive engineering was proposed as an efficient approach to control the nucleation and growth of perovskite crystals. Polymers, macromolecules, and inorganic salts can act as additives or dopants in the perovskite precursor solution.[6,40,52,76,87−89]

Apart from engineering perovskite films, it is also beneficial to modify the surface energy of the underlying layers. Perovskite precursors usually have a poor wetting ability on hydrophobic surfaces of common organic layers, resulting in a smaller number of nucleation sites and thus discontinuous island-like crystal growth. Real-time contact angle results revealed that polyvinyl pyrrolidine (PVP)-modified ZnO films increase surface hydrophilicity, leading to uniform growth of perovskite films with reduced pinholes (Figure 4c). Other organic polymers with hydrophilic surfaces like poly[(9,9-

https://dx.doi.org/10.1021/acsphotonics.0c01394
ACS Photonics 2021, 8, 386−404

bis(3′-(N,N-dimethylamino)propyl)-2,7-fluorene)-alt-2,7-(9,9-dioctylfluorene)] (PFN) and betaine were also successfully introduced as interlayers to improve interfacial contact between HTLs and perovskite layers.[90,91] The interfacial layers can reduce luminescence quenching and decrease energy barrier for charge injection as well. The perovskite film on top of ZnO showed significantly enhanced PL after PVP modification.[72] Polyethylenimine (PEI)-modified ZnO films not only showed better wettability, but also decreased work function of ZnO from 3.7 to 3.2 eV, reducing the energy barrier for electron injection.[92,93]

Extract Light from PeLEDs More Efficiently. While the internal PLQYs of perovskites are already approaching their full potential,[3−5,94] the studies on light outcoupling of PeLEDs have just began. If we look back to the progress on OLEDs and QLEDs, research efforts are devoted to material development at the beginning, but once materials have been developed to maturity, researchers focus on light extraction. PeLEDs are likely to follow the same trend. The refractive indices of perovskites (≈2.6 for $MAPbI_3$) are usually higher than those of organic emitters (<1.8).[95] As a result, the waveguided mode of the generated light can be a major optical energy loss in PeLEDs due to total internal reflection (TIR) at the interfaces of perovskite emitters, limiting the light outcoupling efficiency to 20−30% (Figure 4d).[78,96] This highlights the importance of light extraction management for PeLEDs and leaves considerable opportunities for efficiency improvement. Several general strategies can be considered to improve light extraction from PeLEDs.

First, a simple approach is to adhere an index-matched half-ball lens or a microlens array to the substrate, which can efficiently extract the light trapped in the substrate mode without altering angular emission profiles.[97,98] Second, significant optical energy losses in waveguide mode can be minimized by embedding patterned nanostructures in functional layers. This approach has been well-established in OLEDs in which Qu et al. demonstrated that a nondiffractive dielectric grid layer placed between the transparent anode and the substrate could couple out all waveguided light into the substrate without changing the device electrical properties.[99] Similar approaches have been applied in PeLEDs,[100−102] Shen et al. integrated bioinspired moth eye nanostructures into a ZnO layer to reduce the waveguided light loss.[102] The EQE was improved from 13.4% for the planar PeLED to 20.4% for the patterned PeLED. Combining with a glass half-ball lens, they achieved a record-high EQE of 28.2% for PeLEDs at that time.

However, these photonic nanostructures usually require complicated fabrication procedures, which may not be practically suited for manufacturing. Therefore, the third strategy, engineering the morphologies and optoelectronic properties of perovskite films, could be a cost-effective option. Cao et al. demonstrated that spontaneously formed submicrometer-scale structures in solution-processed perovskite films could improve light outcoupling from PeLEDs.[17] Zhao et al. showed the optimal outcoupling efficiency occurs with perovskite thicknesses in the range of 35−40 nm.[103] The optical simulation reveals the light interference effect exists in the PeLED cavity, the outcoupling efficiency shows an oscillating behavior when the thickness of the perovskite layer varies. The transitional dipole moment orientation also plays an important role in light extraction (Figure 4e).[96] Vertically orientated dipoles mainly emit light traveling with a large angle to the surface normal, which can be easily trapped inside the device stack.[104] Therefore, horizontally oriented dipoles are preferred over vertically oriented dipoles. The fraction of horizontal dipoles to total dipoles can be defined as α, and it is equal to 0.67 in the isotropic dipole case as two-thirds of emissions come from the in-plane (horizontal) dipoles. Recent reports show $CsPbBr_3$ nanoplate films have an increased α value when the thickness decreases, which is due to the progressive confinement of excitons within the nanoplates.[96,105,106] Similarly, 2D layered perovskite films show a high α value (around 0.8) due to the in-plane confinement within 2D structures. In contrast, 3D bulk films show a more isotropic emission ($\alpha \approx 0.6$).[107,108] By virtue of high α, it is possible for quasi-2D PeLEDs to have a higher outcoupling efficiency than 3D counterparts. However, it should be noted that the dipole orientation is also highly dependent on film morphology, crystal structure, and dielectric environment.[96,105−107]

At last, perovskites usually have relatively small Stokes-shifts (strong overlap between absorption and emission spectra) and sufficiently high radiation efficiency, which leads to the occurrence of substantial photon recycling (PR).[109] If nonradiative processes can be substantially suppressed, photons absorbed in the emitter are reemitted without loss, increasing the probability to leave the device.[77] The process of PR can be useful for extracting trapped light in the perovskite layer as this provides the opportunity for a large fraction of waveguide photons to be reemitted and outcoupled to the air. Cho et al. showed that PR can contribute more than 70% to the overall emission (Figure 4f).[95] Taking the PR phenomenon into consideration, they showed that PeLEDs can achieve a maximum EQE of 100% theoretically for a perfect IQE. However, parasitic absorption loss from metal electrodes becomes an important limiting factor and prevents PeLEDs from achieving this theoretical efficiency. Practically, the maximum achievable EQE is restricted to between 20% and 25% in current PeLED architectures. However, this value can be further increased by maximizing PR, for example, increasing the reabsorption and PLQY. A dedicated design of nanostructured electrodes with reduced electrode areas can be utilized to minimize parasitic absorption.[95] Compared to OLEDs where the emitters usually have large Stokes-shift, attention to photon recycling can improve efficiency in PeLEDs.

CURRENT STAGE OF HYBRID PEROVSKITE LASERS AND FUTURE OPPORTUNITIES

Why Hybrid Perovskite Emitters Are Excellent Gain Media. Over the past several decades, solution-processed semiconductor emitters have gathered much attention and experienced sufficient development in LED and laser applications. However, researchers are still looking for a low cost, solution-processable, flexible material capable of electrically pumped lasing. Leading contenders include organic semiconductors, inorganic colloidal nanocrystals and now hybrid perovskites.[110] Achieving CW lasing under optical pumping is regarded as an important step toward electrically pumped lasing. However, it still remains a challenging objective for the organic semiconductor family,[111] colloidal nanocrystals only made this step recently, almost two decades after initial investigations.[112−114] Nevertheless, further progress toward the electrically pumped lasing is expected to be highly

https://dx.doi.org/10.1021/acsphotonics.0c01394
ACS Photonics 2021, 8, 386−404

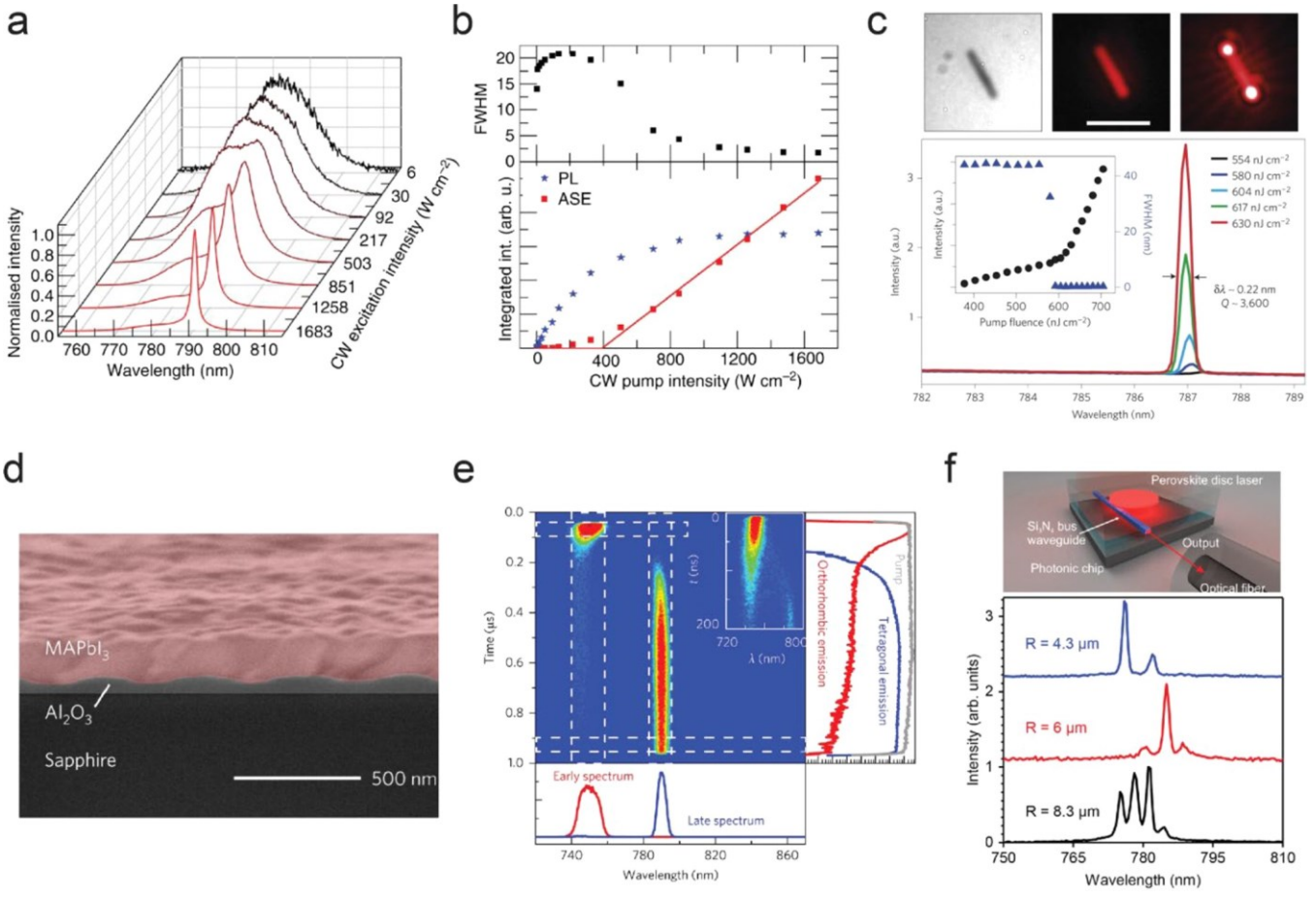

Figure 5. Amplified spontaneous emission and population inversion lasing based on perovskite emitters. (a) The emission spectrum evolution from a broadband PL spectrum (fwhm ~ 15−20 nm) to a narrowband ASE spectrum (fwhm ~ 2 nm) with increasing excitation intensities. (b) PL, ASE, and fwhm as a function of the CW excitation intensity, the CW ASE threshold is 387 W cm^{-2}. (c) NW emission spectra around the lasing threshold. Inset: Integrated emission intensity and fwhm as a function of P showing the lasing threshold at 600 nJ cm^{-2}. Top: fluorescent images of a NW at different excitation fluence. (d) Cross-sectional SEM image of the second-order DFB laser architecture. (e) Streak camera image of ASE emission from the $MAPbI_3$ film optically pumped by 920 ns-long pulses when the substrate temperature is lowered to T = 106 K. (f) Schematic device structure of the perovskite disk laser, and lasing spectra with varying disk radii at excitation of 1.15 × P_{th}. (a, b) Reprinted with permission from ref 23. Copyright 2019 Springer Nature. (c) Reprinted with permission from ref 121. Copyright 2015 Springer Nature. (d, e) Reprinted with permission from ref 24. Copyright 2017 Springer Nature. (f) Reprinted with permission from ref 137. Copyright 2018 American Chemical Society.

challenging for colloidal NCs due to their limited charge transport properties from insulating ligands.

A well-known issue with organic lasers is triplet accumulation.[115] The radiative decay of triplets in organic semiconductors is generally spin-forbidden and thus extremely slow (microseconds or longer). Once a molecule is in the triplet state, it is no longer available for stimulated emission.[116] It appears that triplet accumulation is less of an issue for perovskite lasers, at least for some certain types of perovskites.[116] Becker et al. have demonstrated the strong spin−orbit coupling combined with the Rashba effect could lead to highly emissive triplet states in cesium lead halide perovskites, which is a unique advantage for achieving CW lasing.[117] As a result, very recently, Qin et al. achieved CW lasing in quasi-2D perovskite films at room temperature, which is encouraging news in the perovskite laser community.

Compared to other solution-processed materials, although perovskites exhibit similar thermal conductivity values, they possess much higher carrier mobilities (e.g., perovskite single crystals have shown ultrahigh carrier mobilities of 190 and 217 cm^2 V^{-1} s^{-1} for electrons and holes, respectively).[110,118] Therefore, the Joule heating in perovskites is lower, and thus, perovskite materials are amenable to higher injection currents. In addition, the facile bandgap tunability of perovskites gain media could enable tunable lasing from UV to NIR spectral regions.

Amplified Spontaneous Emission and Population Inversion Lasing. For the occurrence of ASE, the gain medium needs to be excited by an intense pump to build up population inversion and enable stimulated emission. Xing et al. reported ASE from a 65 nm thick $MAPbI_3$ film at a remarkably low threshold (12 μJ cm^{-2}) in 2014.[119] Since then, intensive research has been devoted to exploring perovskites for lasing applications. CW ASE at low temperatures (T < 120 K) was demonstrated by Brenner et al. by using a triple-cation perovskite $Cs_{0.1}(MA_{0.17}FA_{0.83})_{0.9}Pb_{0.84}(I_{0.84}Br_{0.16})_{2.68}$ (Figure 5a,b). At temperatures higher than 120 K, the material tends to degrade due to the thermal accumulation before the CW ASE threshold is reached. Thermal management is thus further required to overcome this issue and achieve CW lasing at room temperature.[23]

For population inversion lasing, an optical cavity (or resonator) is required to provide optical feedback for laser oscillation. There are mainly two categories of optical cavities:

https://dx.doi.org/10.1021/acsphotonics.0c01394
ACS Photonics 2021, 8, 386−404

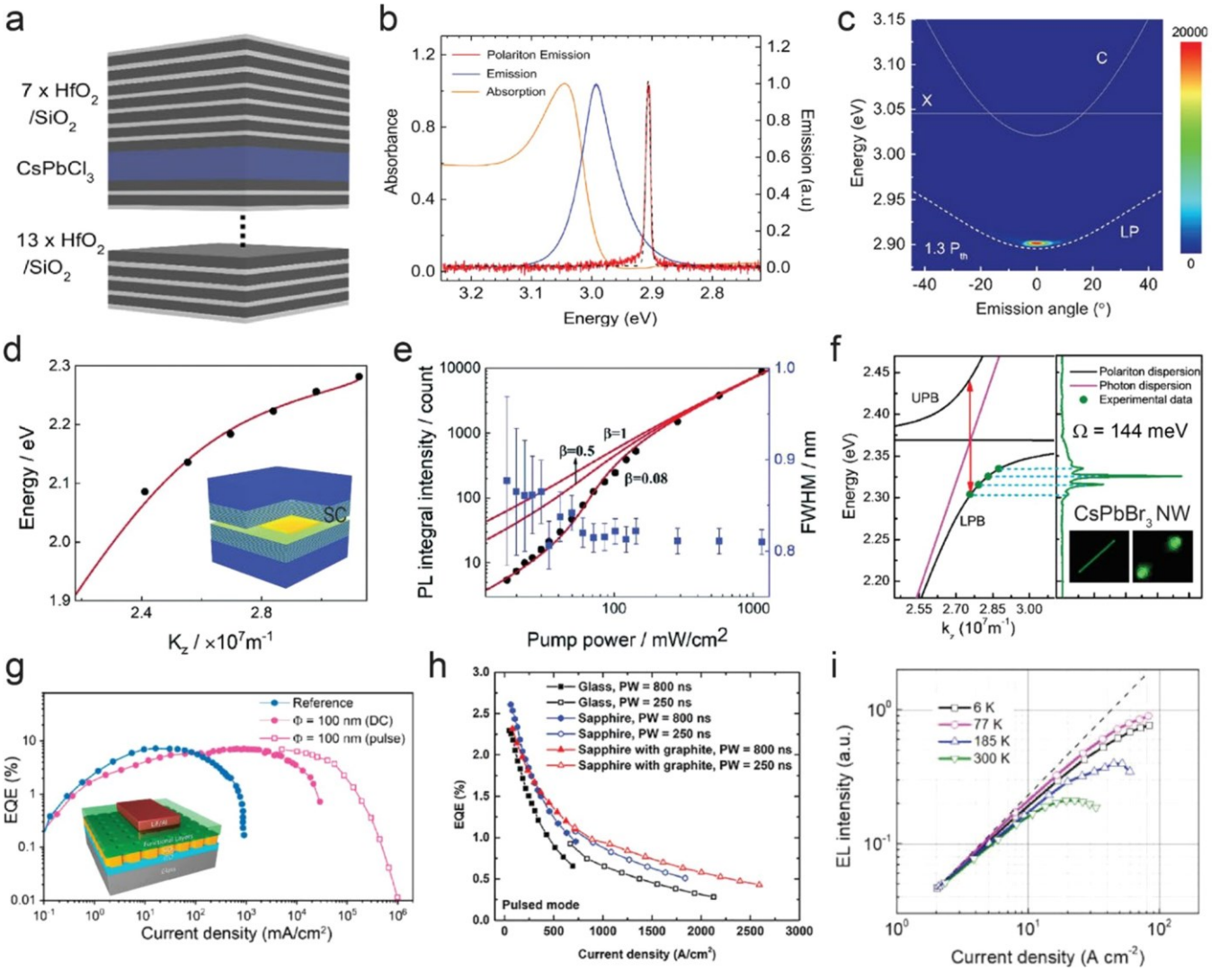

Figure 6. Exciton−polariton lasing and progress toward electrically driven lasers. (a) Schematic architecture of the perovskite microcavity, $CsPbCl_3$ nanoplatelets are embedded in a planar microcavity constituted by a bottom and a top HfO_2/SiO_2 DBR. (b) Room-temperature photoluminescence absorption spectra of the $CsPbCl_3$ nanoplatelets and the polariton emission from the perovskite microcavity. (c) Angle-resolved photoluminescence spectrum measured at 1.3 P_{th}. (d). The lower polariton dispersion curve of the $MAPbBr_3$ single crystal film inside the microcavity. Inset: schematic structure of the perovskite microcavity. (e) The intensity and fwhm of 565 nm peak changes with increasing pump fluences. (f) Dispersion curves of photonic mode (pink line) and exciton-polariton (black line) for the $CsPbBr_3$ NW with a length of ~10 μm. (g) EQE−J curves for reference and nanopatterned PeLEDs. Inset: schematic structure of nanopatterned PeLEDs. (h) EQE−J curves for PeLEDs on glass or sapphire substrates, with or without heat sink, all driven in pulsed mode. (i) Plot of EL intensity as a function of current density at various temperatures from 6 to 300 K. (a−c) Reprinted with permission from ref 141. Copyright 2017 American Chemical Society. (d, e) Reprinted with permission from ref 143. Copyright 2019 Royal Society of Chemistry. (f) Reprinted with permission from ref 145. Copyright 2018 American Chemical Society. (g) Reprinted with permission from ref 53. Copyright 2020 American Chemical Society. (h) Reprinted with permission from ref 148. Copyright 2020 John Wiley and Sons. (i) Reprinted with permission from ref 151. Copyright 2020 American Institute of Physics.

intrinsic and external cavities. The intrinsic cavity is the perovskite medium itself with a particular shape that forms the resonant cavity, like 1D perovskite nanowires (NWs), 2D microdisks, and 3D microsphere. These perovskite nanostructures can be synthesized by liquid-phase self-assembly, liquid−solid interface growth, and vapor-phase growth methods.[120−124] The perovskite NW is intrinsically a Fabry−Perot (FP) cavity with two end-facets as reflectors, and the cavity length is the same as the NW longitudinal length (Figure 5c).[121] 2D microdisks and 3D microspheres can constitute whispering-gallery-mode (WGM) cavities with crystal lateral surfaces as reflectors to provide optical resonance. The spectral spacing between lasing modes is highly dependent on the structure geometry.[125] Although WGM cavities can have extremely high Q factors intrinsically (on the order of 10^8), the Q factors of perovskite WGM lasers (only $10^3−10^4$) are mostly limited by the scattering loss of perovskite films.[125−127]

The external cavity represents an additional geometry that provides optical feedback, including distributed Bragg reflector (DBR), distributed feedback (DFB), photonic crystal (PC), and WGM cavities. The DBR is a dielectric mirror consisting of multiple pairs of alternative layers with different refractive indices. The perovskite gain medium is embedded between bottom and top DBR mirrors (or a top metal mirror) to form the vertical-cavity surface emitting laser (VCSEL). The number of lasing peaks in a VCSEL depends on the overlap

https://dx.doi.org/10.1021/acsphotonics.0c01394
ACS Photonics 2021, 8, 386−404

between the resonance modes supported by the DBR cavity and the spectral region of optical gain. Hence, single-mode lasing usually requires a short cavity length.[128,129]

The DFB cavity is composed of a periodically structured element, which acts as a distributed reflector in the wavelength range of laser action. Compared to DBR and FP lasers, DFB lasers are more stable and able to achieve single-frequency and high-power laser beams. 1D Bragg diffraction grating and 2D PC are the most common DFB cavities exploited in perovskite lasers. For a 1D Bragg diffraction grating, the resonant wavelength is given by Bragg conditions described as[130]

$$2n_{\text{eff}}\Lambda = m\lambda_{\text{Bragg}} \quad (5)$$

where n_{eff} is the effective refractive index of the integrated structure, Λ is the grating period, m is the diffraction order, and λ_{Bragg} is the Bragg wavelength. The first- (m = 1) and second-order (m = 2) Bragg diffractions lead to edge- and surface-emitting DFB lasers, respectively.

Jia et al. achieved a CW-pumped $MAPbI_3$ DFB laser with a threshold of 17 kW/cm^2 at temperatures below the tetragonal-to-orthorhombic phase transition (T < 160 K).[24] They deposited the $MAPbI_3$ film onto a second-order Al_2O_3 grating on a high thermal-conductivity sapphire substrate and cooled the device to around 100 K (Figure 5d). Tetragonal-phase inclusions formed inside the bulk orthorhombic host matrix within a few 100 ns upon intense optical excitation, presumably due to local heating (Figure 5e). The mixed-phase system creates a transient energy landscape for excitons that is analogous to inorganic quantum wells or organic host−guest matrices, thus, can avoid the lasing death phenomenon for pure tetragonal phase and lead to continuous gain.[116] Although this demonstration of CW lasing was an impressive achievement, the requirement for the mixed phase system is not very practical. Later, Jia et al. showed that the lasing ceases under CW operation stem from pump-induced heating and photoinduced defects that increase nonradiative Shockley-Read-Hall rates.[131] They predicted that the threshold of current DFB lasers must be decreased by an order of magnitude to achieve CW operation at room temperature.

Apart from planar microcavities, the microspheres, capillaries, and ring resonators can function as external WGM microcavities.[132−136] WGM cavities possess many unique properties, such as ultrahigh Q-factors, low mode volumes, small sizes of resonators, and ease of fabrication. However, they also usually lead to isotropic laser output, which is not favorable when integrating with other optical components. Cegielski et al. reported a ring resonator composed of a perovskite disc and a Si_3N_4 bus waveguide (Figure 5f).[137] Effective coupling between the perovskite microdisk and Si_3N_4 waveguide enables the directional laser output from the outcoupling Si_3N_4 waveguide.

Exciton−Polariton Lasing Requires Reduced Threshold. Compared to conventional population inversion lasing, exciton−polariton lasing is expected to require a lower threshold. The strong coupling between electron−hole pairs (excitons) and photons confined in an optical microcavity leads to the formation of Bosonic quasi-particles, known as exciton−polaritons.[138] Polariton lasers are based on the Bose−Einstein condensation (BEC) of cavity exciton−polaritons, where a large number of Bosons condense into the lowest quantum state and leak coherent photons upon reaching a critical threshold.[139] The exciton−photon coupling strength in an optical cavity can be described by the Rabi splitting energy (Ω), which is a function of oscillator numbers per volume (n), oscillator strength (f), and mode volume (V_m) as $\Omega \sim \sqrt{nf/V_m}$.[140] According to the equation, the coupling strength can be enhanced via (1) increasing the number of oscillators by improving Q factor of optical cavities; (2) boosting oscillator strength by increasing exciton binding energy; and (3) reducing mode volume of optical cavities.

Halide perovskites are ideal materials for exciton−polariton lasing due to their modest exciton binding energy and coulomb interactions.[130] Perovskite polariton lasing has been demonstrated by Su et al. using a $CsPbCl_3$ nanoplate embedded DBR cavity (Figure 6a,b).[141] The CVD-grown $CsPbCl_3$ nanoplates were selected as the active material because of the large exciton binding energy (72 meV) and high crystal quality.[142] The highly reflective DBR mirrors can form a high-Q optical cavity. Above the threshold, the ground state near the minimum of lower polariton dispersion becomes macroscopically occupied, confirming polariton condensation and subsequent polariton lasing (Figure 6c). Recently, Tian et al. reported CW lasing in a perovskite single crystal VCSEL at room temperature (Figure 6d,e).[143] The authors attributed the extremely low CW-lasing threshold (34 mW/cm^2) to a high-quality perovskite single crystal, low loss DBR cavity, and possible occurrence of polariton lasing in the strongly confined optical cavity. Although the authors observed a large Rabi splitting energy of 372 meV at room temperature, further support for polariton lasing in this work are in investigation.

Besides DBR cavities, perovskite NW cavities have also been widely used in exciton−polariton lasing benefiting from the ease of fabrication.[138,140,144,145] Coupling between light and the exciton resonance is enhanced in a NW cavity due to the reduced mode volume and the cavity enhanced oscillator strength.[144] Wang et al. reported exciton−polariton lasing from all-inorganic perovskite NWs.[145] The energy of the lasing peaks for $CsPbBr_3$ NWs (green scatter dots) is well fitted by the exciton−polariton model and situated on the lower polariton branch (Figure 6f). A large Rabi splitting energy of 210 ± 13, 146 ± 9, and 103 ± 5 meV was observed for $CsPbCl_3$, $CsPbBr_3$, and $CsPbI_3$ NWs, respectively, which follows the same trend as exciton binding energy of these NWs. The findings of perovskite polariton lasing may push forward the development of optically pumped CW and electrically driven lasers.

Toward Electrically Driven Perovskite Lasers. A long-standing and elusive goal in solution-processed optoelectronics is the development of an electrically driven laser. By virtue of superior optoelectronic properties, perovskites renewed researchers' hope for achieving this long-standing goal. An electrically driven perovskite laser device would require (1) incorporation of well-designed optical resonant cavity to reduce the lasing threshold, external cavities like DFB and DBR are preferred as the fabrication process would be nonintrusive. The impact to perovskite films should be minimized. (2) A highly efficient LED structure, which can be injected with intense current and meanwhile the emission-quenching process is suppressed. The purpose is to increase the product of current density (J) and EQE.[146]

Typically, the required J × EQE to achieve electrically pumped lasing of perovskites is estimated to be tens of A/cm^2.[53,147,148] Currently, although the peak EQEs of PeLEDs have reached over 20%, they are usually achieved at J < 100 mA/cm^2. The EQEs start to drop significantly at high J, a

https://dx.doi.org/10.1021/acsphotonics.0c01394
ACS Photonics 2021, 8, 386−404

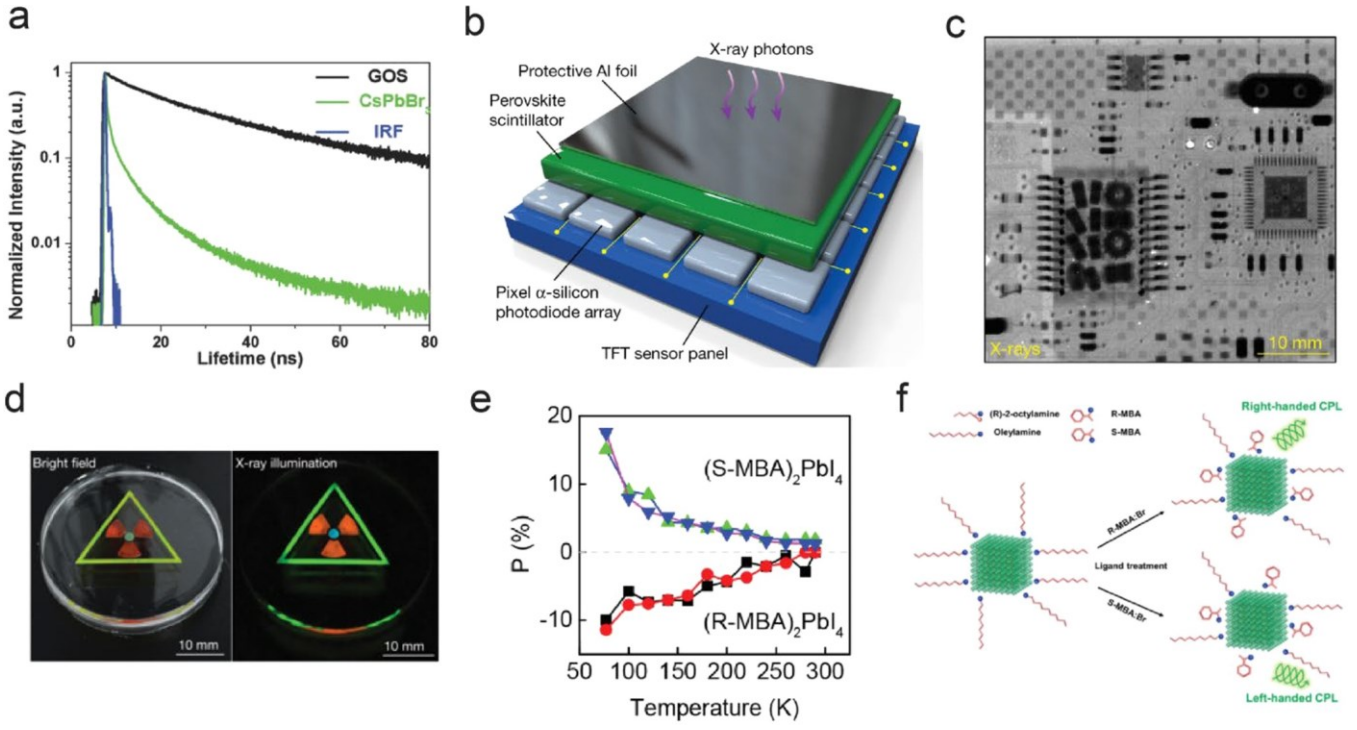

Figure 7. Perovskite emitters for applications of X-ray scintillation and circularly polarized light sources. (a) Dynamic PL decay spectra for lifetime measurement of $CsPbBr_3$ NCs and conventional GOS scintillators. (b) Multilayered design of the flat-panel X-ray imaging system based on $CsPbBr_3$ NCs. (c) X-ray image of a network interface card obtained using the flat-panel detector in (b). (d) Multicolor X-ray scintillation from three types of perovskite nanocrystal scintillators. (e) Degree of circularly polarized PL (P) as a function of temperature for chiral 2D perovskites. (f) Postsynthetic ligand treatment of $FAPbBr_3$ NCs with R-,S-MBA:Br. (a) Reprinted with permission from ref 161. Copyright 2018 John Wiley and Sons. (b−d) Reprinted with permission from ref 159. Copyright 2018 Springer Nature. (e) Reprinted with permission from ref 175. Copyright 2019 American Chemical Society. (f) Reprinted with permission from ref 178. Copyright 2020 American Chemical Society.

phenomenon termed as efficiency roll-off or droop. To reach the lasing threshold, it becomes necessary for developing a PeLED which can tolerate a high J over several hundreds of A/cm^2. At such a high J, Joule heating would become a severe problem given the relatively low thermal conductivity (i.e., $MAPbI_3 \sim 1.8\ Wm^{-1}\ K^{-1}$ for pseudocubic phase).[149] Several strategies have been proposed for effective thermal management very recently. First, substrates with higher thermal conductivity such as sapphire and silicon could be used to take replace conventional glass substrates.[53,150] Second, graphite and diamond heat sink adhered to top metal electrodes of PeLEDs could further dissipate Joule heat.[148] Third, reduced device geometry with patterned current apertures could help dissipate Joule heat to surrounding areas.[53,148] At last, pulsed current operation helps devices survive at higher J by further reducing the average heating rate. Exploiting combined strategies, the maximum J × EQE values of 2.1 and 10 A/cm^2 have been achieved for green and near-infrared PeLEDs, respectively (Figure 6g,h).[53,148] PeLEDs that can operate at 2.5 kA/cm^2 and maintain an EQE of 1% at 1 kA/cm^2 were achieved.[148] The cryostat-temperature operation may be able to further improve the J × EQE value (Figure 6i).[151]

As we have mentioned in LEDs Exploiting Perovskite Emitters, balancing charge injection is effective to suppress efficiency roll-off. Herein, we want to further emphasize that Auger recombination can also contribute to efficiency roll-off. Auger recombination becomes prominent at high charge carrier densities. Huang group suggested the efficiency roll-off in their quasi-2D PeLEDs is likely from Auger recombination.[33] In quasi-2D perovskites, the charge carriers are concentrated in the QWs. As a result, local carrier densities in the QWs of quasi-2D perovskites are much higher than those of 3D perovskites, the Auger process thus becomes more important at relatively lower carrier densities. The specific point at which Auger recombination dominates has received some controversy as Kim et al. show high current densities exceeding 150 A/cm^2 without the effect, and thus, this point requires more insight.[147]

In future work toward electrically driven perovskite lasers, more research is needed for demonstrating PeLEDs with simultaneous high EQE and brightness. Both parameters are important in display and lighting applications. At the same time, incorporating a well-designed cavity to increase the light−matter interaction is also warranted. Since exciton−polariton lasing does not require population inversion and presents a lower lasing threshold, electrically driven polariton lasers could be an interesting field to explore. As the electrical pulse duration is typically longer than the optical pulse, it will be helpful to find perovskite emitters that have low ASE thresholds and can persist lasing under long-pulse pumping (microsecond level).

MORE APPLICATIONS OF HYBRID PEROVSKITE EMITTERS

Perovskite Scintillators for X-ray Imaging. In addition to extensive applications in LEDs and lasers, hybrid perovskites have recently gathered much attention in the field of X-ray detections, due to their strong X-ray stopping capacity, high detection sensitivity, excellent charge transport properties, and low-cost solution-processability. The applications of X-ray

https://dx.doi.org/10.1021/acsphotonics.0c01394
ACS Photonics 2021, 8, 386−404

detectors are ubiquitous in our daily life, such as medical diagnosis, safety inspection, and metal crack detection.[152] At present, two methods prevail in detecting X-ray. The domination method is based on indirect detection using scintillators to convert X-ray photons to lower-energy photons (UV−visible-NIR) that can be detected by photodetectors. Commonly used scintillators include thallium-doped cesium iodide (Cs:Tl) and terbium-doped gadolinium oxysulfide (Gd_2O_2S:Tb, GOS:Tb). The other method is based on direct detection using direct photoconductors such as amorphous selenium (a-Se) to convert X-ray photons to electron−hole pairs that can be collected under electric bias. This method is particularly suitable for high-resolution applications like mammography.

To fulfill the predominant task of X-ray imaging, large-area flat panel detectors (FPDs) are demanded. Kim et al. reported first large-area perovskite X-ray imager in 2017, which provides at least 10-fold higher sensitivity compared to currently used a-Se or CsI:Tl detectors.[153] They printed an 830 μm thick polycrystalline $MAPbI_3$ film as the direct X-ray converter on a thin-film transistor (TFT) plane. However, this perovskite X-ray imager also presented about a two-order higher dark current and relative slower response time compared to stabilized a-Se detectors. Furthermore, the relatively high signal crosstalk between pixels lead to worse spatial resolution, presumably caused by $MAPbI_3$ crystallites of 20−200 μm sizes that are larger than a pixel and can overlap neighboring pixels. Therefore, certain technological challenges remain to be addressed for direct-type perovskite X-ray detectors.

In comparison to direct perovskite X-ray converters, the development of perovskite scintillators appears more competitive in the current market situation, presumably due to ease of fabrication on commercial platforms, faster scintillation response, and weaker requirements for charge transport properties.[152] To improve the X-ray absorption coefficient (μ) and reduce scintillator thickness, materials with a high density (ρ) and a high atomic number (Z) are preferred as $\mu \propto \frac{\rho Z^4}{E^3}$, where E is the X-ray photon energy. Since common elements in the halide perovskite material system, for example, Cs, Pb, Bi, Br, and I, have high Z, halide perovskites are thus very suited for X-ray scintillators.[154] Perovskite single crystals have exhibited respectable scintillation behaviors but only at a very low temperature (<130 K);[155] the light yields of methylammonium lead halide crystals are less than 1000 photons/MeV at room temperature.[156] 2D layered perovskites have shown higher light yields of 9000−14000 photons/MeV benefiting from reduced dimensionality.[156−158] Similarly, $CsPbBr_3$ nanocrystals have been reported to possess a high light yield of 33000 photons/MeV.[159,160] Among commercially available scintillators, only CsI:Tl shows a higher light yield than $CsPbBr_3$ NCs (1.85-fold).[159] However, unlike CsI:Tl scintillators, which typically have the issue of afterglow luminescence due to long scintillation decay time (1000 ns), perovskite NCs exhibit a very fast response (44.6 ns) to X-rays, making them suitable candidates for high-speed and real-time X-ray imaging applications.[159] Heo et al. compared $CsPbBr_3$ NCs with conventional GOS:Tb scintillators. The PeNCs exhibited about 3-fold higher light yield compared to GOS:Tb and a 5.6-fold faster photoluminescence lifetime (Figure 7a).[161] The superior radioluminescence and accelerated radiative decay time from perovskite NC scintillators are due to the large exciton binding energy originated from quantum confinement and bright triplet states without accumulating charge carriers.[117] Operational stability issues associated with ion migrations in perovskite photovoltaic and LED applications could be largely avoided in X-ray scintillation settings.

Perovskite NCs show comparable photostability to commercial scintillators under X-ray excitation, potentially enabling commercialized applications of perovskite X-ray detectors.[161] Based on the superior optoelectronic properties of perovskite NCs, large area FPDs based on indirect X-ray converters of perovskite NCs have been successfully demonstrated (Figure 7b,c).[159,161] The perovskite NC films with sufficient thickness could be easily integrated with a-Si photodetector arrays due to the facile solution-processability. The demonstrated $CsPbBr_3$ NC FPDs exhibit much higher spatial resolution than those of commercially used CsI:Tl and GOS:Tb based FPDs, which is likely due to the lower degree of light scattering in perovskite NC films with monodispersed cubic shape and uniform NC size, compared to commercial bulk scintillators made of polycrystalline ceramics or column pillars. To further reduce signal crosstalk, perovskite NC films could be patterned by photolithography to form column scintillators, mimicking the current design of multicolumn scintillators made of vacuum evaporated CsI:Tl to mitigate waveguide effects.[160,162] Although there is still much work to be done on material optimization, we believe large-area perovskite NC scintillators can offer great potential for next-generation industrial X-ray sensors and imagers.

Another unique advantage of hybrid perovskites NCs compared to other scintillators is the facile tunability of X-ray excited emission wavelengths through tailoring the halide composition and NC size. This advantage offers the opportunity to achieve multicolor scintillation based on perovskite NC scintillators (Figure 7d). The emission wavelengths of perovskite NCs can cover a wide spectral range from UV to NIR. Lanthanide ions (Yb^{3+}, Er^{3+}, Eu^{3+}, Ce^{3+}) doped perovskite NCs are an emerging material family that has attracted growing interest.[163,164] The Yb^{3+}-doped $CsPbCl_3$ NCs could achieve over 100% PLQY, which is particularly favorable for X-ray scintillators. Excited electrons in $CsPbCl_3$ can be divided to excite two Yb^{3+} ions, leading to blue and NIR (over 1000 nm) emission simultaneously.[165] In addition, lanthanide elements have very high atomic number, the doping of lanthanide ions could increase the X-ray absorption coefficient.

Circularly Polarized Light Sources. Perovskite emitters also possess advantages as light sources of circularly polarized luminescence (CPL), which could be used in various future technologies.[166−168] Perovskites have large spin−orbit coupling and Rashba splitting due to their high Z atoms, making manipulation of the spin freedom in the emitting states possible and thus can emit CPL. External magnetic field can induce splitting of spin momentum in $MAPbI_3$ crystals, generating CPL at low temperature.[169,170] The excellent tunability of dimensionality, composition and crystal forms of perovskites can increase the degree of CPL ($[PL(\sigma+) - PL(\sigma-)]/[PL(\sigma+) + PL(\sigma-)]$) and induce the CPL emission even without magnetic field. Perovskites show controllable spin coherence lifetime when changing the dimensionality and halide anion, which indicates that CPL intensity can be further enhanced.[171−173] Chiral organic A-site cation molecules, such as chiral R,S-methylbenzylammonium (R,S-MBA), can be incorporated into the layered perovskite polycrystalline bulk films and induce asymmetric structural arrangement of Pb-X

https://dx.doi.org/10.1021/acsphotonics.0c01394
ACS Photonics 2021, 8, 386−404

inorganic lattices.[174] The chiral (R-,S-MBA)$_2$PbI$_4$ single crystals exhibit a maximum degree of CPL of 17.6% at 77 K (Figure 7e).[175]

Chiral organic molecules can also induce CPL from colloidal perovskite NCs at room temperature without magnetic field by attaching on the NC surfaces or inducing assembly of nanocrystals.[176,177] Very recently, chiral (R)-2-octylamine was used to modify the size, surface chemistry, and photophysical properties of colloidal organic−inorganic FAPbBr$_3$ nanocrystals and achieve CPL from the NCs.[178,179] Furthermore, chiral R-,S-MBA bromide (R,S-MBA:Br) salts were introduced to the nanocrystals after purification and achieved CPL from purified nanocrystals, providing a way to demonstrate the spintronic devices based on colloidal perovskite NCs (Figure 7f).

CONCLUSION AND PROSPECTS

Due to the accumulated knowledge and experience in the longstanding development of organics and colloidal nanocrystals, the progress in the field of light emission with halide perovskites has been remarkably rapid. This exciting family of materials with outstanding optoelectronic properties holds great promise to break into the field previously dominated by other materials. Currently, lead-based perovskites still prevail due to their superior properties; however, this may cause environmental concerns, given the toxicity of lead. Further identification of Pb-free light emitters or on-chip sequestration of Pb is a critical area of focus.[180,181]

Through engineering control of excitonic recombination, energy funneling, and surface defects, perovskite emitters have exhibited high PLQYs approaching 100%, which forms a firm foundation on the booming development of PeLEDs. Green, red, and NIR PeLEDs have achieved high EQEs of more than 20%, through multiple strategies, including charge injection balance, morphology control, and light extraction management, demonstrating great potential for natural-color displays.[182] However, the development of blue PeLEDs still lags because of poor film quality and deficient device structure, which demands additional effort as blue LEDs are essential for displays and lighting. Meanwhile, PeLEDs still face device stability issues toward commercialized applications. Currently, the lifetimes and stability of PeLEDs remain far from satisfactory: about 250 h of operation in air before a 50% luminescence reduction.[39,183] Ion migration, electrochemical reactions, and interfacial reactions are regarded as the main degradation pathways affecting the operational stability.[26]

For solution-processed lasing, the "holy grail" is an electrically driven laser. The achievement of CW perovskite lasing paves the way toward this long-standing goal. Besides remarkable performance in conventional population-inversion lasing, perovskite emitters provide an alternative pathway for a low-threshold lasing via exciton−polaritons, which is promising for developing an electrically driven perovskite laser. Other novel applications of perovskite emitters, such as X-ray scintillation, chiral light sources have also been thriving, and more applications (e.g., color converters, single photon emitters, etc.) are expected to disrupt mainstream manufacturing in the field of light-emission in the near future.

AUTHOR INFORMATION

Corresponding Authors

Lih Y. Lin − Department of Electrical and Computer Engineering, University of Washington, Seattle, Washington 98195, United States; orcid.org/0000-0001-9748-5478; Email: lylin@uw.edu

Joseph M. Luther − Chemical and Materials Science, National Renewable Energy Laboratory (NREL), Golden, Colorado 80401, United States; orcid.org/0000-0002-4054-8244; Email: joey.luther@nrel.gov

Authors

Chen Zou − Department of Electrical and Computer Engineering, University of Washington, Seattle, Washington 98195, United States; Chemical and Materials Science, National Renewable Energy Laboratory (NREL), Golden, Colorado 80401, United States; orcid.org/0000-0001-9638-6363

Congyang Zhang − Department of Electrical and Computer Engineering, University of Washington, Seattle, Washington 98195, United States

Young-Hoon Kim − Chemical and Materials Science, National Renewable Energy Laboratory (NREL), Golden, Colorado 80401, United States; orcid.org/0000-0003-1810-6885

Complete contact information is available at: https://pubs.acs.org/10.1021/acsphotonics.0c01394

Notes

The authors declare no competing financial interest.

ACKNOWLEDGMENTS

This work was authored in part by the National Renewable Energy Laboratory, operated by Alliance for Sustainable Energy, LLC, for the U.S. Department of Energy (DOE) under Contract No. DE-AC36-08GO28308. Y.-H.K. and J.M.L. acknowledge the Center for Hybrid Organic Inorganic Semiconductors for Energy (CHOISE), an Energy Frontier Research Center funded by the Office of Basic Energy Sciences, Office of Science, within the U.S. Department of Energy. The views expressed in the article do not necessarily represent the views of the DOE or the U.S. Government. C.Z., C.Z., and L.Y.L. acknowledge the funding support from the National Science Foundation (Grant # ECCS-1807397 and INTERN Program) and the University of Washington Royalty Research Fund.

REFERENCES

(1) Kojima, A.; Teshima, K.; Shirai, Y.; Miyasaka, T. Organometal halide perovskites as visible-light sensitizers for photovoltaic cells. J. Am. Chem. Soc. 2009, 131, 6050−6051.

(2) NREL Best Research-Cell Efficiencies, https://www.nrel.gov/pv/assets/pdfs/best-research-cell-efficiencies.20190802.pdf.

(3) Zheng, X.; Yuan, S.; Liu, J.; Yin, J.; Yuan, F.; Shen, W.-S.; Yao, K.; Wei, M.; Zhou, C.; Song, K.; Zhang, B.-B.; Lin, Y.; Hedhili, M. N.; Wehbe, N.; Han, Y.; Sun, H.-T.; Lu, Z.-H.; Anthopoulos, T. D.; Mohammed, O. F.; Sargent, E. H.; Liao, L.-S.; Bakr, O. M. Chlorine Vacancy Passivation in Mixed Halide Perovskite Quantum Dots by Organic Pseudohalides Enables Efficient Rec. 2020 Blue Light-Emitting Diodes. ACS Energy Lett. 2020, 5, 793−798.

(4) Abdi-Jalebi, M.; Andaji-Garmaroudi, Z.; Cacovich, S.; Stavrakas, C.; Philippe, B.; Richter, J. M.; Alsari, M.; Booker, E. P.; Hutter, E. M.; Pearson, A. J.; Lilliu, S.; Savenije, T. J.; Rensmo, H.; Divitini, G.; Ducati, C.; Friend, R. H.; Stranks, S. D. Maximizing and Stabilizing Luminescence from Halide Perovskites with Potassium Passivation. Nature 2018, 555, 497−501.

(5) Braly, I. L.; DeQuilettes, D. W.; Pazos-Outon, L. M.; Burke, S.; Ziffer, M. E.; Ginger, D. S.; Hillhouse, H. W. Hybrid Perovskite Films

Approaching the Radiative Limit with over 90% Photoluminescence Quantum Efficiency. Nat. Photonics 2018, 12, 355−361.
(6) Zhao, B.; Bai, S.; Kim, V.; Lamboll, R.; Shivanna, R.; Auras, F.; Richter, J. M.; Yang, L.; Dai, L.; Alsari, M.; She, X.-J.; Liang, L.; Zhang, J.; Lilliu, S.; Gao, P.; Snaith, H. J.; Wang, J.; Greenham, N. C.; Friend, R. H.; Di, D. High-Efficiency Perovskite-Polymer Bulk Heterostructure Light-Emitting Diodes. Nat. Photonics 2018, 12, 783−789.
(7) Herz, L. M. Charge-Carrier Mobilities in Metal Halide Perovskites: Fundamental Mechanisms and Limits. ACS Energy Lett. 2017, 2, 1539−1548.
(8) Wehrenfennig, C.; Eperon, G. E.; Johnston, M. B.; Snaith, H. J.; Herz, L. M. High charge carrier mobilities and lifetimes in organolead trihalide perovskites. Adv. Mater. 2014, 26, 1584−1589.
(9) Lu, M.; Zhang, Y.; Wang, S.; Guo, J.; Yu, W. W.; Rogach, A. L. Metal Halide Perovskite Light-Emitting Devices: Promising Technology for Next-Generation Displays. Adv. Funct. Mater. 2019, 29, 1902008.
(10) Kim, Y. H.; Kim, J. S.; Lee, T. W. Strategies to Improve Luminescence Efficiency of Metal-Halide Perovskites and Light-Emitting Diodes. Adv. Mater. 2019, 31, 1804595.
(11) Kim, Y. H.; Kim, S.; Jo, S. H.; Lee, T. W. Metal Halide Perovskites: From Crystal Formations to Light-Emitting-Diode Applications. Small Methods 2018, 2, 1800093.
(12) Zhao, X.; Ng, J. D. A.; Friend, R. H.; Tan, Z.-K. Opportunities and Challenges in Perovskite Light-Emitting Devices. ACS Photonics 2018, 5, 3866−3875.
(13) Jean, J.; Xiao, J.; Nick, R.; Moody, N.; Nasilowski, M.; Bawendi, M.; Bulović, V. Synthesis cost dictates the commercial viability of lead sulfide and perovskite quantum dot photovoltaics. Energy Environ. Sci. 2018, 11, 2295−2305.
(14) Tan, Z. K.; Moghaddam, R. S.; Lai, M. L.; Docampo, P.; Higler, R.; Deschler, F.; Price, M.; Sadhanala, A.; Pazos, L. M.; Credgington, D.; Hanusch, F.; Bein, T.; Snaith, H. J.; Friend, R. H. Bright light-emitting diodes based on organometal halide perovskite. Nat. Nanotechnol. 2014, 9, 687−692.
(15) Lin, K.; Xing, J.; Quan, L. N.; de Arquer, F. P. G.; Gong, X.; Lu, J.; Xie, L.; Zhao, W.; Zhang, D.; Yan, C.; Li, W.; Liu, X.; Lu, Y.; Kirman, J.; Sargent, E. H.; Xiong, Q.; Wei, Z. Perovskite Light-Emitting Diodes with External Quantum Efficiency Exceeding 20 Per Cent. Nature 2018, 562, 245−248.
(16) Xu, W.; Hu, Q.; Bai, S.; Bao, C.; Miao, Y.; Yuan, Z.; Borzda, T.; Barker, A. J.; Tyukalova, E.; Hu, Z.; Kawecki, M.; Wang, H.; Yan, Z.; Liu, X.; Shi, X.; Uvdal, K.; Fahlman, M.; Zhang, W.; Duchamp, M.; Liu, J.-M.; Petrozza, A.; Wang, J.; Liu, L.-M.; Huang, W.; Gao, F. Rational molecular passivation for high-performance perovskite light-emitting diodes. Nat. Photonics 2019, 13, 418−424.
(17) Cao, Y.; Wang, N.; Tian, H.; Guo, J.; Wei, Y.; Chen, H.; Miao, Y.; Zou, W.; Pan, K.; He, Y.; Cao, H.; Ke, Y.; Xu, M.; Wang, Y.; Yang, M.; Du, K.; Fu, Z.; Kong, D.; Dai, D.; Jin, Y.; Li, G.; Li, H.; Peng, Q.; Wang, J.; Huang, W. Perovskite Light-Emitting Diodes Based on Spontaneously Formed Submicrometre-Scale Structures. Nature 2018, 562, 249−253.
(18) Yuan, M.; Quan, L. N.; Comin, R.; Walters, G.; Sabatini, R.; Voznyy, O.; Hoogland, S.; Zhao, Y.; Beauregard, E. M.; Kanjanaboos, P.; Lu, Z.; Kim, D. H.; Sargent, E. H. Perovskite energy funnels for efficient light-emitting diodes. Nat. Nanotechnol. 2016, 11, 872−877.
(19) Wang, N.; Cheng, L.; Ge, R.; Zhang, S.; Miao, Y.; Zou, W.; Yi, C.; Sun, Y.; Cao, Y.; Yang, R.; Wei, Y.; Guo, Q.; Ke, Y.; Yu, M.; Jin, Y.; Liu, Y.; Ding, Q.; Di, D.; Yang, L.; Xing, G.; Tian, H.; Jin, C.; Gao, F.; Friend, R. H.; Wang, J.; Huang, W. Perovskite light-emitting diodes based on solution-processed self-organized multiple quantum wells. Nat. Photonics 2016, 10, 699−704.
(20) Wang, Q.; Wang, X.; Yang, Z.; Zhou, N.; Deng, Y.; Zhao, J.; Xiao, X.; Rudd, P.; Moran, A.; Yan, Y.; Huang, J. Efficient Sky-Blue Perovskite Light-Emitting Diodes via Photoluminescence Enhancement. Nat. Commun. 2019, 10, 5633.
(21) Chiba, T.; Hayashi, Y.; Ebe, H.; Hoshi, K.; Sato, J.; Sato, S.; Pu, Y.-J.; Ohisa, S.; Kido, J. Anion-Exchange Red Perovskite Quantum Dots with Ammonium Iodine Salts for Highly Efficient Light-Emitting Devices. Nat. Photonics 2018, 12, 681−687.
(22) Dong, Y.; Wang, Y.-K.; Yuan, F.; Johnston, A.; Liu, Y.; Ma, D.; Choi, M.-J.; Chen, B.; Chekini, M.; Baek, S.-W.; Sagar, L. K.; Fan, J.; Hou, Y.; Wu, M.; Lee, S.; Sun, B.; Hoogland, S.; Quintero-Bermudez, R.; Ebe, H.; Todorovic, P.; Dinic, F.; Li, P.; Kung, H. T.; Saidaminov, M. I.; Kumacheva, E.; Spiecker, E.; Liao, L.-S.; Voznyy, O.; Lu, Z.-H.; Sargent, E. H. Bipolar-shell resurfacing for blue LEDs based on strongly confined perovskite quantum dots. Nat. Nanotechnol. 2020, 15, 668−674.
(23) Brenner, P.; Bar-On, O.; Jakoby, M.; Allegro, I.; Richards, B. S.; Paetzold, U. W.; Howard, I. A.; Scheuer, J.; Lemmer, U. Continuous Wave Amplified Spontaneous Emission in Phase-Stable Lead Halide Perovskites. Nat. Commun. 2019, 10, 988.
(24) Jia, Y.; Kerner, R. A.; Grede, A. J.; Rand, B. P.; Giebink, N. C. Continuous-Wave Lasing in an Organic-Inorganic Lead Halide Perovskite Semiconductor. Nat. Photonics 2017, 11, 784−788.
(25) Qin, C.; Sandanayaka, A. S. D.; Zhao, C.; Matsushima, T.; Zhang, D.; Fujihara, T.; Adachi, C. Stable room-temperature continuous-wave lasing in quasi-2D perovskite films. Nature 2020, 585, 53−57.
(26) Dong, Q.; Lei, L.; Mendes, J.; So, F. Operational stability of perovskite light emitting diodes. J. Phys. Mater. 2020, 3, 012002.
(27) Cho, H.; Kim, Y. H.; Wolf, C.; Lee, H. D.; Lee, T. W. Improving the Stability of Metal Halide Perovskite Materials and Light-Emitting Diodes. Adv. Mater. 2018, 30, 1704587.
(28) Lee, H.; Ko, D.; Lee, C. Direct Evidence of Ion-Migration-Induced Degradation of Ultrabright Perovskite Light-Emitting Diodes. ACS Appl. Mater. Interfaces 2019, 11, 11667−11673.
(29) Xing, G.; Wu, B.; Wu, X.; Li, M.; Du, B.; Wei, Q.; Guo, J.; Yeow, E. K.; Sum, T. C.; Huang, W. Transcending the Slow Bimolecular Recombination in Lead-Halide Perovskites for Electroluminescence. Nat. Commun. 2017, 8, 14558.
(30) Milot, R. L.; Eperon, G. E.; Green, T.; Snaith, H. J.; Johnston, M. B.; Herz, L. M. Radiative Monomolecular Recombination Boosts Amplified Spontaneous Emission in $HC(NH2)_2SnI_3$ Perovskite Films. J. Phys. Chem. Lett. 2016, 7, 4178−4184.
(31) Crothers, T. W.; Milot, R. L.; Patel, J. B.; Parrott, E. S.; Schlipf, J.; Muller-Buschbaum, P.; Johnston, M. B.; Herz, L. M. Photon Reabsorption Masks Intrinsic Bimolecular Charge-Carrier Recombination in CH3NH3PbI3 Perovskite. Nano Lett. 2017, 17, 5782−5789.
(32) Chen, Z.; Li, Z.; Zhang, C.; Jiang, X. F.; Chen, D.; Xue, Q.; Liu, M.; Su, S.; Yip, H. L.; Cao, Y. Recombination Dynamics Study on Nanostructured Perovskite Light-Emitting Devices. Adv. Mater. 2018, 30, 1801370.
(33) Zou, W.; Li, R.; Zhang, S.; Liu, Y.; Wang, N.; Cao, Y.; Miao, Y.; Xu, M.; Guo, Q.; Di, D.; Zhang, L.; Yi, C.; Gao, F.; Friend, R. H.; Wang, J.; Huang, W. Minimising Efficiency Roll-Off in High-Brightness Perovskite Light-Emitting Diodes. Nat. Commun. 2018, 9, 608.
(34) Miyata, A.; Mitioglu, A.; Plochocka, P.; Portugall, O.; Wang, J. T.-W.; Stranks, S. D.; Snaith, H. J.; Nicholas, R. J. Direct measurement of the exciton binding energy and effective masses for charge carriers in organic−inorganic tri-halide perovskites. Nat. Phys. 2015, 11, 582−587.
(35) Yang, Y.; Yan, Y.; Yang, M.; Choi, S.; Zhu, K.; Luther, J. M.; Beard, M. C. Low Surface Recombination Velocity in Solution-Grown $CH_3NH_3PbBr_3$ Perovskite Single Crystal. Nat. Commun. 2015, 6, 7961.
(36) DeQuilettes, D. W.; Koch, S.; Burke, S.; Paranji, R. K.; Shropshire, A. J.; Ziffer, M. E.; Ginger, D. S. Photoluminescence Lifetimes Exceeding 8 μs and Quantum Yields Exceeding 30% in Hybrid Perovskite Thin Films by Ligand Passivation. ACS Energy Lett. 2016, 1, 438−444.
(37) Sum, T. C.; Righetto, M.; Lim, S. S. Quo vadis, perovskite emitters? J. Chem. Phys. 2020, 152, 130901.
(38) Cho, H.; Jeong, S.-H.; Park, M.-H.; Kim, Y.-H.; Wolf, C.; Lee, C.-L.; Heo, J. H.; Sadhanala, A.; Myoung, N.; Yoo, S.; Im, S. H.; Friend, R. H.; Lee, T.-W. Overcoming the Electroluminescence

https://dx.doi.org/10.1021/acsphotonics.0c01394
ACS Photonics 2021, 8, 386−404

Efficiency Limitations of Perovskite Light-Emitting Diodes. Science 2015, 350, 1222−1225.
(39) Wang, H.; Zhang, X.; Wu, Q.; Cao, F.; Yang, D.; Shang, Y.; Ning, Z.; Zhang, W.; Zheng, W.; Yan, Y.; Kershaw, S. V.; Zhang, L.; Rogach, A. L.; Yang, X. Trifluoroacetate induced small-grained CsPbBr3 perovskite films result in efficient and stable light-emitting devices. Nat. Commun. 2019, 10, 665.
(40) Ling, Y.; Tian, Y.; Wang, X.; Wang, J. C.; Knox, J. M.; Perez-Orive, F.; Du, Y.; Tan, L.; Hanson, K.; Ma, B.; Gao, H. Enhanced Optical and Electrical Properties of Polymer-Assisted All-Inorganic Perovskites for Light-Emitting Diodes. Adv. Mater. 2016, 28, 8983−8989.
(41) Zhang, F.; Zhong, H.; Chen, C.; Wu, X.-g.; Hu, X.; Huang, H.; Han, J.; Zou, B.; Dong, Y. Brightly luminescent and color-tunable colloidal $CH_3NH_3PbX_3$ (X= Br, I, Cl) quantum dots: potential alternatives for display technology. ACS Nano 2015, 9, 4533−4542.
(42) Protesescu, L.; Yakunin, S.; Bodnarchuk, M. I.; Krieg, F.; Caputo, R.; Hendon, C. H.; Yang, R. X.; Walsh, A.; Kovalenko, M. V. Nanocrystals of Cesium Lead Halide Perovskites (CsPbX3, X = Cl, Br, and I): Novel Optoelectronic Materials Showing Bright Emission with Wide Color Gamut. Nano Lett. 2015, 15, 3692−3696.
(43) Gao, X.; Zhang, X.; Yin, W.; Wang, H.; Hu, Y.; Zhang, Q.; Shi, Z.; Colvin, V. L.; Yu, W. W.; Zhang, Y. Ruddlesden-Popper Perovskites: Synthesis and Optical Properties for Optoelectronic Applications. Adv. Sci. 2019, 6, 1900941.
(44) Cheng, L.; Jiang, T.; Cao, Y.; Yi, C.; Wang, N.; Huang, W.; Wang, J. Multiple-Quantum-Well Perovskites for High-Performance Light-Emitting Diodes. Adv. Mater. 2020, 32, 1904163.
(45) Quan, L. N.; Zhao, Y.; Garcia de Arquer, F. P.; Sabatini, R.; Walters, G.; Voznyy, O.; Comin, R.; Li, Y.; Fan, J. Z.; Tan, H.; Pan, J.; Yuan, M.; Bakr, O. M.; Lu, Z.; Kim, D. H.; Sargent, E. H. Tailoring the Energy Landscape in Quasi-2D Halide Perovskites Enables Efficient Green-Light Emission. Nano Lett. 2017, 17, 3701−3709.
(46) Fu, W.; Liu, H.; Shi, X.; Zuo, L.; Li, X.; Jen, A. K. Y. Tailoring the Functionality of Organic Spacer Cations for Efficient and Stable Quasi-2D Perovskite Solar Cells. Adv. Funct. Mater. 2019, 29, 1900221.
(47) Yuan, S.; Wang, Z. K.; Xiao, L. X.; Zhang, C. F.; Yang, S. Y.; Chen, B. B.; Ge, H. T.; Tian, Q. S.; Jin, Y.; Liao, L. S. Optimization of Low-Dimensional Components of Quasi-2D Perovskite Films for Deep-Blue Light-Emitting Diodes. Adv. Mater. 2019, 31, 1904319.
(48) Qin, C.; Matsushima, T.; Potscavage, W. J.; Sandanayaka, A. S. D.; Leyden, M. R.; Bencheikh, F.; Goushi, K.; Mathevet, F.; Heinrich, B.; Yumoto, G.; Kanemitsu, Y.; Adachi, C. Triplet management for efficient perovskite light-emitting diodes. Nat. Photonics 2020, 14, 70−75.
(49) Lee, S.; Park, J. H.; Lee, B. R.; Jung, E. D.; Yu, J. C.; Di Nuzzo, D.; Friend, R. H.; Song, M. H. Amine-Based Passivating Materials for Enhanced Optical Properties and Performance of Organic-Inorganic Perovskites in Light-Emitting Diodes. J. Phys. Chem. Lett. 2017, 8, 1784−1792.
(50) Yang, X.; Zhang, X.; Deng, J.; Chu, Z.; Jiang, Q.; Meng, J.; Wang, P.; Zhang, L.; Yin, Z.; You, J. Efficient Green Light-Emitting Diodes Based on Quasi-Two-Dimensional Composition and Phase Engineered Perovskite with Surface Passivation. Nat. Commun. 2018, 9, 570.
(51) Wang, H.; Kosasih, F. U.; Yu, H.; Zheng, G.; Zhang, J.; Pozina, G.; Liu, Y.; Bao, C.; Hu, Z.; Liu, X.; Kobera, L.; Abbrent, S.; Brus, J.; Jin, Y.; Fahlman, M.; Friend, R. H.; Ducati, C.; Liu, X.-K.; Gao, F. Perovskite-molecule composite thin films for efficient and stable light-emitting diodes. Nat. Commun. 2020, 11, 891.
(52) Wu, T.; Li, J.; Zou, Y.; Xu, H.; Wen, K.; Wan, S.; Bai, S.; Song, T.; McLeod, J. A.; Duhm, S.; Gao, F.; Sun, B. High-Performance Perovskite Light-Emitting Diode with Enhanced Operational Stability Using Lithium Halide Passivation. Angew. Chem., Int. Ed. 2020, 59, 4099−4105.
(53) Zou, C.; Liu, Y.; Ginger, D. S.; Lin, L. Y. Suppressing Efficiency Roll-Off at High Current Densities for Ultra-Bright Green Perovskite Light-Emitting Diodes. ACS Nano 2020, 14, 6076−6086.
(54) Fang, Z.; Chen, W.; Shi, Y.; Zhao, J.; Chu, S.; Zhang, J.; Xiao, Z. Dual Passivation of Perovskite Defects for Light-Emitting Diodes with External Quantum Efficiency Exceeding 20%. Adv. Funct. Mater. 2020, 30, 1909754.
(55) Zhang, T.; Xie, L.; Chen, L.; Guo, N.; Li, G.; Tian, Z.; Mao, B.; Zhao, Y. In Situ Fabrication of Highly Luminescent Bifunctional Amino Acid Crosslinked 2D/3D $NH_3C_4H_9COO(CH_3NH_3PbBr_3)_n$ Perovskite Films. Adv. Funct. Mater. 2017, 27, 1603568.
(56) Pan, J.; Quan, L. N.; Zhao, Y.; Peng, W.; Murali, B.; Sarmah, S. P.; Yuan, M.; Sinatra, L.; Alyami, N. M.; Liu, J.; Yassitepe, E.; Yang, Z.; Voznyy, O.; Comin, R.; Hedhili, M. N.; Mohammed, O. F.; Lu, Z. H.; Kim, D. H.; Sargent, E. H.; Bakr, O. M. Highly Efficient Perovskite-Quantum-Dot Light-Emitting Diodes by Surface Engineering. Adv. Mater. 2016, 28, 8718−8725.
(57) Tan, Y.; Zou, Y.; Wu, L.; Huang, Q.; Yang, D.; Chen, M.; Ban, M.; Wu, C.; Wu, T.; Bai, S.; Song, T.; Zhang, Q.; Sun, B. Highly Luminescent and Stable Perovskite Nanocrystals with Octylphosphonic Acid as a Ligand for Efficient Light-Emitting Diodes. ACS Appl. Mater. Interfaces 2018, 10, 3784−3792.
(58) Pan, J.; Shang, Y.; Yin, J.; De Bastiani, M.; Peng, W.; Dursun, I.; Sinatra, L.; El-Zohry, A. M.; Hedhili, M. N.; Emwas, A. H.; Mohammed, O. F.; Ning, Z.; Bakr, O. M. Bidentate Ligand-Passivated CsPbI3 Perovskite Nanocrystals for Stable Near-Unity Photoluminescence Quantum Yield and Efficient Red Light-Emitting Diodes. J. Am. Chem. Soc. 2018, 140, 562−565.
(59) Yang, D.; Li, X.; Zhou, W.; Zhang, S.; Meng, C.; Wu, Y.; Wang, Y.; Zeng, H. $CsPbBr_3$ Quantum Dots 2.0: Benzenesulfonic Acid Equivalent Ligand Awakens Complete Purification. Adv. Mater. 2019, 31, 1900767.
(60) Koscher, B. A.; Swabeck, J. K.; Bronstein, N. D.; Alivisatos, A. P. Essentially Trap-Free $CsPbBr_3$ Colloidal Nanocrystals by Postsynthetic Thiocyanate Surface Treatment. J. Am. Chem. Soc. 2017, 139, 6566−6569.
(61) Li, F.; Liu, Y.; Wang, H.; Zhan, Q.; Liu, Q.; Xia, Z. Postsynthetic Surface Trap Removal of CsPbX3 (X = Cl, Br, or I) Quantum Dots via a ZnX2/Hexane Solution toward an Enhanced Luminescence Quantum Yield. Chem. Mater. 2018, 30, 8546−8554.
(62) Yang, J.-N.; Song, Y.; Yao, J.-S.; Wang, K.-H.; Wang, J.-J.; Zhu, B.-S.; Yao, M.-M.; Rahman, S. U.; Lan, Y.-F.; Fan, F.-J.; Yao, H.-B. Potassium Bromide Surface Passivation on $CsPbI_{3-x}Br_x$ Nanocrystals for Efficient and Stable Pure Red Perovskite Light-Emitting Diodes. J. Am. Chem. Soc. 2020, 142, 2956−2967.
(63) Na Quan, L.; Ma, D.; Zhao, Y.; Voznyy, O.; Yuan, H.; Bladt, E.; Pan, J.; García de Arquer, F. P.; Sabatini, R.; Piontkowski, Z.; Emwas, A.-H.; Todorović, P.; Quintero-Bermudez, R.; Walters, G.; Fan, J. Z.; Liu, M.; Tan, H.; Saidaminov, M. I.; Gao, L.; Li, Y.; Anjum, D. H.; Wei, N.; Tang, J.; McCamant, D. W.; Roeffaers, M. B. J.; Bals, S.; Hofkens, J.; Bakr, O. M.; Lu, Z.-H.; Sargent, E. H. Edge Stabilization in Reduced-Dimensional Perovskites. Nat. Commun. 2020, 11, 170.
(64) Saidaminov, M. I.; Kim, J.; Jain, A.; Quintero-Bermudez, R.; Tan, H.; Long, G.; Tan, F.; Johnston, A.; Zhao, Y.; Voznyy, O.; Sargent, E. H. Suppression of atomic vacancies via incorporation of isovalent small ions to increase the stability of halide perovskite solar cells in ambient air. Nature Energy 2018, 3, 648−654.
(65) Gangishetty, M. K.; Sanders, S. N.; Congreve, D. N. Mn^{2+} Doping Enhances the Brightness, Efficiency, and Stability of Bulk Perovskite Light-Emitting Diodes. ACS Photonics 2019, 6, 1111−1117.
(66) Bechtel, J. S.; Van der Ven, A. Octahedral tilting instabilities in inorganic halide perovskites. Physical Review Materials 2018, 2, 025401.
(67) Mondal, N.; De, A.; Samanta, A. Achieving Near-Unity Photoluminescence Efficiency for Blue-Violet-Emitting Perovskite Nanocrystals. ACS Energy Lett. 2019, 4, 32−39.
(68) Lu, M.; Zhang, X.; Zhang, Y.; Guo, J.; Shen, X.; Yu, W. W.; Rogach, A. L. Simultaneous Strontium Doping and Chlorine Surface Passivation Improve Luminescence Intensity and Stability of $CsPbI_3$ Nanocrystals Enabling Efficient Light-Emitting Devices. Adv. Mater. 2018, 30, 1804691.

https://dx.doi.org/10.1021/acsphotonics.0c01394
ACS Photonics 2021, 8, 386−404

(69) Yong, Z. J.; Guo, S. Q.; Ma, J. P.; Zhang, J. Y.; Li, Z. Y.; Chen, Y. M.; Zhang, B. B.; Zhou, Y.; Shu, J.; Gu, J. L.; Zheng, L. R.; Bakr, O. M.; Sun, H. T. Doping-Enhanced Short-Range Order of Perovskite Nanocrystals for Near-Unity Violet Luminescence Quantum Yield. J. Am. Chem. Soc. 2018, 140, 9942−9951.
(70) Zou, S.; Liu, Y.; Li, J.; Liu, C.; Feng, R.; Jiang, F.; Li, Y.; Song, J.; Zeng, H.; Hong, M.; Chen, X. Stabilizing cesium lead halide perovskite lattice through Mn(II) substitution for air-stable light-emitting diodes. J. Am. Chem. Soc. 2017, 139, 11443−11450.
(71) Cho, H.; Kim, J. S.; Wolf, C.; Kim, Y. H.; Yun, H. J.; Jeong, S. H.; Sadhanala, A.; Venugopalan, V.; Choi, J. W.; Lee, C. L.; Friend, R. H.; Lee, T. W. High-Efficiency Polycrystalline Perovskite Light-Emitting Diodes Based on Mixed Cations. ACS Nano 2018, 12, 2883−2892.
(72) Zhang, L.; Yang, X.; Jiang, Q.; Wang, P.; Yin, Z.; Zhang, X.; Tan, H.; Yang, Y. M.; Wei, M.; Sutherland, B. R.; Sargent, E. H.; You, J. Ultra-Bright and Highly Efficient Inorganic Based Perovskite Light-Emitting Diodes. Nat. Commun. 2017, 8, 15640.
(73) Shynkarenko, Y.; Bodnarchuk, M. I.; Bernasconi, C.; Berezovska, Y.; Verteletskyi, V.; Ochsenbein, S. T.; Kovalenko, M. V. Direct Synthesis of Quaternary Alkylammonium-Capped Perovskite Nanocrystals for Efficient Blue and Green Light-Emitting Diodes. ACS Energy Lett. 2019, 4, 2703−2711.
(74) Xing, J.; Zhao, Y.; Askerka, M.; Quan, L. N.; Gong, X.; Zhao, W.; Zhao, J.; Tan, H.; Long, G.; Gao, L.; Yang, Z.; Voznyy, O.; Tang, J.; Lu, Z. H.; Xiong, Q.; Sargent, E. H. Color-Stable Highly Luminescent Sky-Blue Perovskite Light-Emitting Diodes. Nat. Commun. 2018, 9, 3541.
(75) Jiang, Y.; Qin, C.; Cui, M.; He, T.; Liu, K.; Huang, Y.; Luo, M.; Zhang, L.; Xu, H.; Li, S.; Wei, J.; Liu, Z.; Wang, H.; Kim, G.-H.; Yuan, M.; Chen, J. Spectra stable blue perovskite light-emitting diodes. Nat. Commun. 2019, 10, 1868.
(76) Ban, M.; Zou, Y.; Rivett, J. P. H.; Yang, Y.; Thomas, T. H.; Tan, Y.; Song, T.; Gao, X.; Credgington, D.; Deschler, F.; Sirringhaus, H.; Sun, B. Solution-Processed Perovskite Light Emitting Diodes with Efficiency Exceeding 15% through Additive-Controlled Nanostructure Tailoring. Nat. Commun. 2018, 9, 3892.
(77) Stranks, S. D.; Hoye, R. L. Z.; Di, D.; Friend, R. H.; Deschler, F. The Physics of Light Emission in Halide Perovskite Devices. Adv. Mater. 2019, 31, 1803336.
(78) Shi, X.-B.; Liu, Y.; Yuan, Z.; Liu, X.-K.; Miao, Y.; Wang, J.; Lenk, S.; Reineke, S.; Gao, F. Optical Energy Losses in Organic-Inorganic Hybrid Perovskite Light-Emitting Diodes. Adv. Opt. Mater. 2018, 6, 1800667.
(79) Lu, M.; Guo, J.; Sun, S.; Lu, P.; Wu, J.; Wang, Y.; Kershaw, S. V.; Yu, W. W.; Rogach, A. L.; Zhang, Y. Bright CsPbI3 Perovskite Quantum Dot Light-Emitting Diodes with Top-Emitting Structure and a Low Efficiency Roll-Off Realized by Applying Zirconium Acetylacetonate Surface Modification. Nano Lett. 2020, 20, 2829−2836.
(80) Yang, X.; Chu, Z.; Meng, J.; Yin, Z.; Zhang, X.; Deng, J.; You, J. Effects of Organic Cations on the Structure and Performance of Quasi-Two-Dimensional Perovskite-Based Light-Emitting Diodes. J. Phys. Chem. Lett. 2019, 10, 2892−2897.
(81) Fakharuddin, A.; Qiu, W.; Croes, G.; Devizis, A.; Gegevicius, R.; Vakhnin, A.; Rolin, C.; Genoe, J.; Gehlhaar, R.; Kadashchuk, A.; Gulbinas, V.; Heremans, P. Reduced Efficiency Roll-Off and Improved Stability of Mixed 2D/3D Perovskite Light Emitting Diodes by Balancing Charge Injection. Adv. Funct. Mater. 2019, 29, 1904101.
(82) Kim, Y. H.; Cho, H.; Heo, J. H.; Kim, T. S.; Myoung, N.; Lee, C. L.; Im, S. H.; Lee, T. W. Multicolored organic/inorganic hybrid perovskite light-emitting diodes. Adv. Mater. 2015, 27, 1248−1254.
(83) Wang, Y.; Teng, Y.; Lu, P.; Shen, X.; Jia, P.; Lu, M.; Shi, Z.; Dong, B.; Yu, W. W.; Zhang, Y. Low Roll-Off Perovskite Quantum Dot Light-Emitting Diodes Achieved by Augmenting Hole Mobility. Adv. Funct. Mater. 2020, 30, 1910140.
(84) Zhang, X.; Wu, G.; Fu, W.; Qin, M.; Yang, W.; Yan, J.; Zhang, Z.; Lu, X.; Chen, H. Orientation Regulation of Phenylethylammonium Cation Based 2D Perovskite Solar Cell with Efficiency Higher Than 11%. Adv. Energy. Mater. 2018, 8, 1702498.
(85) Eperon, G. E.; Burlakov, V. M.; Docampo, P.; Goriely, A.; Snaith, H. J. Morphological Control for High Performance, Solution-Processed Planar Heterojunction Perovskite Solar Cells. Adv. Funct. Mater. 2014, 24, 151−157.
(86) Jeon, N. J.; Noh, J. H.; Kim, Y. C.; Yang, W. S.; Ryu, S.; Seok, S. I. Solvent engineering for high-performance inorganic-organic hybrid perovskite solar cells. Nat. Mater. 2014, 13, 897−903.
(87) Cheng, L.-P.; Huang, J.-S.; Shen, Y.; Li, G.-P.; Liu, X.-K.; Li, W.; Wang, Y.-H.; Li, Y.-Q.; Jiang, Y.; Gao, F.; Lee, C.-S.; Tang, J.-X. Efficient $CsPbBr_3$ Perovskite Light-Emitting Diodes Enabled by Synergetic Morphology Control. Adv. Opt. Mater. 2019, 7, 1801534.
(88) Yu, J. C.; Lee, A.-Y.; Kim, D. B.; Jung, E. D.; Kim, D. W.; Song, M. H. Enhancing the Performance and Stability of Perovskite Nanocrystal Light-Emitting Diodes with a Polymer Matrix. Advanced Materials Technologies 2017, 2, 1700003.
(89) Wu, C.; Wu, T.; Yang, Y.; McLeod, J. A.; Wang, Y.; Zou, Y.; Zhai, T.; Li, J.; Ban, M.; Song, T.; Gao, X.; Duhm, S.; Sirringhaus, H.; Sun, B. Alternative Type Two-Dimensional-Three-Dimensional Lead Halide Perovskite with Inorganic Sodium Ions as a Spacer for High-Performance Light-Emitting Diodes. ACS Nano 2019, 13, 1645−1654.
(90) Zou, Y.; Ban, M.; Yang, Y.; Bai, S.; Wu, C.; Han, Y.; Wu, T.; Tan, Y.; Huang, Q.; Gao, X.; Song, T.; Zhang, Q.; Sun, B. Boosting Perovskite Light-Emitting Diode Performance via Tailoring Interfacial Contact. ACS Appl. Mater. Interfaces 2018, 10, 24320−24326.
(91) Liu, Q.-W.; Yuan, S.; Sun, S.-Q.; Luo, W.; Zhang, Y.-J.; Liao, L.-S.; Fung, M.-K. Interfacial Engineering for Highly Efficient Quasi-Two Dimensional Organic-Inorganic Hybrid Perovskite Light-Emitting Diodes. J. Mater. Chem. C 2019, 7, 4344−4349.
(92) Wang, J.; Wang, N.; Jin, Y.; Si, J.; Tan, Z. K.; Du, H.; Cheng, L.; Dai, X.; Bai, S.; He, H.; Ye, Z.; Lai, M. L.; Friend, R. H.; Huang, W. Interfacial control toward efficient and low-voltage perovskite light-emitting diodes. Adv. Mater. 2015, 27, 2311−2316.
(93) Kim, Y. H.; Han, T. H.; Cho, H.; Min, S. Y.; Lee, C. L.; Lee, T. W. Polyethylene imine as an ideal interlayer for highly efficient inverted polymer light-emitting diodes. Adv. Funct. Mater. 2014, 24, 3808−3814.
(94) Cheng, T.; Qin, C.; Watanabe, S.; Matsushima, T.; Adachi, C. Stoichiometry Control for the Tuning of Grain Passivation and Domain Distribution in Green Quasi-2D Metal Halide Perovskite Films and Light-Emitting Diodes. Adv. Funct. Mater. 2020, 30, 2001816.
(95) Cho, C.; Zhao, B.; Tainter, G. D.; Lee, J. Y.; Friend, R. H.; Di, D.; Deschler, F.; Greenham, N. C. The role of photon recycling in perovskite light-emitting diodes. Nat. Commun. 2020, 11, 611.
(96) Morgenstern, T.; Lampe, C.; Naujoks, T.; Jurow, M.; Liu, Y.; Urban, A. S.; Brütting, W. Elucidating the performance limits of perovskite nanocrystal light emitting diodes. J. Lumin. 2020, 220, 116939.
(97) Park, M. H.; Park, J.; Lee, J.; So, H. S.; Kim, H.; Jeong, S. H.; Han, T. H.; Wolf, C.; Lee, H.; Yoo, S.; Lee, T. W. Efficient Perovskite Light-Emitting Diodes Using Polycrystalline Core−Shell-Mimicked Nanograins. Adv. Funct. Mater. 2019, 29, 1902017.
(98) Qu, Y.; Kim, J.; Coburn, C.; Forrest, S. R. Efficient, Nonintrusive Outcoupling in Organic Light Emitting Devices Using Embedded Microlens Arrays. ACS Photonics 2018, 5, 2453−2458.
(99) Qu, Y.; Slootsky, M.; Forrest, S. R. Enhanced light extraction from organic light-emitting devices using a sub-anode grid. Nat. Photonics 2015, 9, 758−763.
(100) Jeon, S.; Zhao, L.; Jung, Y. J.; Kim, J. W.; Kim, S. Y.; Kang, H.; Jeong, J. H.; Rand, B. P.; Lee, J. H. Perovskite Light-Emitting Diodes with Improved Outcoupling Using a High-Index Contrast Nanoarray. Small 2019, 15, 1900135.
(101) Zhang, Q.; Tavakoli, M. M.; Gu, L.; Zhang, D.; Tang, L.; Gao, Y.; Guo, J.; Lin, Y.; Leung, S. F.; Poddar, S.; Fu, Y.; Fan, Z. Efficient metal halide perovskite light-emitting diodes with significantly

https://dx.doi.org/10.1021/acsphotonics.0c01394
ACS Photonics 2021, 8, 386−404

improved light extraction on nanophotonic substrates. Nat. Commun. 2019, 10, 727.
(102) Shen, Y.; Cheng, L. P.; Li, Y. Q.; Li, W.; Chen, J. D.; Lee, S. T.; Tang, J. X. Perovskite Light-Emitting Diodes: High-Efficiency Perovskite Light-Emitting Diodes with Synergetic Outcoupling Enhancement. Adv. Mater. 2019, 31, 1970174.
(103) Zhao, L.; Lee, K. M.; Roh, K.; Khan, S. U. Z.; Rand, B. P. Improved Outcoupling Efficiency and Stability of Perovskite Light-Emitting Diodes using Thin Emitting Layers. Adv. Mater. 2019, 31, 1805836.
(104) Schmidt, T. D.; Lampe, T.; Sylvinson, M. R. D.; Djurovich, P. I.; Thompson, M. E.; Brütting, W. Emitter Orientation as a Key Parameter in Organic Light-Emitting Diodes. Phys. Rev. Appl. 2017, 8, 037001.
(105) Jurow, M. J.; Lampe, T.; Penzo, E.; Kang, J.; Koc, M. A.; Zechel, T.; Nett, Z.; Brady, M.; Wang, L. W.; Alivisatos, A. P.; Cabrini, S.; Brutting, W.; Liu, Y. Tunable Anisotropic Photon Emission from Self-Organized $CsPbBr_3$ Perovskite Nanocrystals. Nano Lett. 2017, 17, 4534−4540.
(106) Jurow, M. J.; Morgenstern, T.; Eisler, C.; Kang, J.; Penzo, E.; Do, M.; Engelmayer, M.; Osowiecki, W. T.; Bekenstein, Y.; Tassone, C.; Wang, L. W.; Alivisatos, A. P.; Brutting, W.; Liu, Y. Manipulating the Transition Dipole Moment of $CsPbBr_3$ Perovskite Nanocrystals for Superior Optical Properties. Nano Lett. 2019, 19, 2489−2496.
(107) Walters, G.; Haeberle, L.; Quintero-Bermudez, R.; Brodeur, J.; Kena-Cohen, S.; Sargent, E. H. Directional Light Emission from Layered Metal Halide Perovskite Crystals. J. Phys. Chem. Lett. 2020, 11, 3458−3465.
(108) Zou, C.; Lin, L. Y. Effect of emitter orientation on outcoupling efficiency of perovskite light-emitting diodes. Opt. Lett. 2020, 45, 4786−4789.
(109) Richter, J. M.; Abdi-Jalebi, M.; Sadhanala, A.; Tabachnyk, M.; Rivett, J. P. H.; Pazos-Outon, L. M.; Godel, K. C.; Price, M.; Deschler, F.; Friend, R. H. Enhancing Photoluminescence Yields in Lead Halide Perovskites by Photon Recycling and Light Out-Coupling. Nat. Commun. 2016, 7, 13941.
(110) Sutherland, B. R.; Sargent, E. H. Perovskite photonic sources. Nat. Photonics 2016, 10, 295−302.
(111) Sandanayaka, A. S.; Matsushima, T.; Bencheikh, F.; Yoshida, K.; Inoue, M.; Fujihara, T.; Goushi, K.; Ribierre, J.-C.; Adachi, C. Toward continuous-wave operation of organic semiconductor lasers. Science advances 2017, 3, e1602570.
(112) Grim, J. Q.; Christodoulou, S.; Di Stasio, F.; Krahne, R.; Cingolani, R.; Manna, L.; Moreels, I. Continuous-wave biexciton lasing at room temperature using solution-processed quantum wells. Nat. Nanotechnol. 2014, 9, 891−895.
(113) Fan, F.; Voznyy, O.; Sabatini, R. P.; Bicanic, K. T.; Adachi, M. M.; McBride, J. R.; Reid, K. R.; Park, Y. S.; Li, X.; Jain, A.; Quintero-Bermudez, R.; Saravanapavanantham, M.; Liu, M.; Korkusinski, M.; Hawrylak, P.; Klimov, V. I.; Rosenthal, S. J.; Hoogland, S.; Sargent, E. H. Continuous-wave lasing in colloidal quantum dot solids enabled by facet-selective epitaxy. Nature 2017, 544, 75−79.
(114) Yang, Z.; Pelton, M.; Fedin, I.; Talapin, D. V.; Waks, E. A room temperature continuous-wave nanolaser using colloidal quantum wells. Nat. Commun. 2017, 8, 143.
(115) Kuehne, A. J.; Gather, M. C. Organic Lasers: Recent Developments on Materials, Device Geometries, and Fabrication Techniques. Chem. Rev. 2016, 116, 12823−12864.
(116) Gather, M. C. Continuous lasing for perovskites. Nat. Photonics 2017, 11, 745−747.
(117) Becker, M. A.; Vaxenburg, R.; Nedelcu, G.; Sercel, P. C.; Shabaev, A.; Mehl, M. J.; Michopoulos, J. G.; Lambrakos, S. G.; Bernstein, N.; Lyons, J. L.; Stoferle, T.; Mahrt, R. F.; Kovalenko, M. V.; Norris, D. J.; Raino, G.; Efros, A. L. Bright Triplet Excitons in Caesium Lead Halide Perovskites. Nature 2018, 553, 189−193.
(118) Wei, H.; Fang, Y.; Mulligan, P.; Chuirazzi, W.; Fang, H.-H.; Wang, C.; Ecker, B. R.; Gao, Y.; Loi, M. A.; Cao, L.; Huang, J. Sensitive X-ray detectors made of methylammonium lead tribromide perovskite single crystals. Nat. Photonics 2016, 10, 333−339.
(119) Xing, G.; Mathews, N.; Lim, S. S.; Yantara, N.; Liu, X.; Sabba, D.; Gratzel, M.; Mhaisalkar, S.; Sum, T. C. Low-temperature solution-processed wavelength-tunable perovskites for lasing. Nat. Mater. 2014, 13, 476−480.
(120) Schlaus, A. P.; Spencer, M. S.; Miyata, K.; Liu, F.; Wang, X.; Datta, I.; Lipson, M.; Pan, A.; Zhu, X. Y. How lasing happens in $CsPbBr_3$ perovskite nanowires. Nat. Commun. 2019, 10, 265.
(121) Zhu, H.; Fu, Y.; Meng, F.; Wu, X.; Gong, Z.; Ding, Q.; Gustafsson, M. V.; Trinh, M. T.; Jin, S.; Zhu, X. Y. Lead halide perovskite nanowire lasers with low lasing thresholds and high quality factors. Nat. Mater. 2015, 14, 636−642.
(122) Zhou, H.; Yuan, S.; Wang, X.; Xu, T.; Wang, X.; Li, H.; Zheng, W.; Fan, P.; Li, Y.; Sun, L.; Pan, A. Vapor growth and tunable lasing of band gap engineered cesium lead halide perovskite micro/nanorods with triangular cross section. ACS Nano 2017, 11, 1189−1195.
(123) Tang, B.; Dong, H.; Sun, L.; Zheng, W.; Wang, Q.; Sun, F.; Jiang, X.; Pan, A.; Zhang, L. Single-Mode Lasers Based on Cesium Lead Halide Perovskite Submicron Spheres. ACS Nano 2017, 11, 10681−10688.
(124) Liao, Q.; Hu, K.; Zhang, H.; Wang, X.; Yao, J.; Fu, H. Perovskite Microdisk Microlasers Self-Assembled from Solution. Adv. Mater. 2015, 27, 3405−3410.
(125) Wang, K.; Wang, S.; Xiao, S.; Song, Q. Recent Advances in Perovskite Micro- and Nanolasers. Adv. Opt. Mater. 2018, 6, 1800278.
(126) Wang, S.; Liu, Y.; Li, G.; Zhang, J.; Zhang, N.; Xiao, S.; Song, Q. Lead Halide Perovskite Based Microdisk Lasers for On-Chip Integrated Photonic Circuits. Adv. Opt. Mater. 2018, 6, 1701266.
(127) Zhang, N.; Sun, W.; Rodrigues, S. P.; Wang, K.; Gu, Z.; Wang, S.; Cai, W.; Xiao, S.; Song, Q. Highly Reproducible Organometallic Halide Perovskite Microdevices based on Top-Down Lithography. Adv. Mater. 2017, 29, 1606205.
(128) Wang, Y.; Li, X.; Nalla, V.; Zeng, H.; Sun, H. Solution-Processed Low Threshold Vertical Cavity Surface Emitting Lasers from All-Inorganic Perovskite Nanocrystals. Adv. Funct. Mater. 2017, 27, 1605088.
(129) Huang, C.-Y.; Zou, C.; Mao, C.; Corp, K. L.; Yao, Y.-C.; Lee, Y.-J.; Schlenker, C. W.; Jen, A. K. Y.; Lin, L. Y. $CsPbBr_3$ Perovskite Quantum Dot Vertical Cavity Lasers with Low Threshold and High Stability. ACS Photonics 2017, 4, 2281−2289.
(130) Dong, H.; Zhang, C.; Liu, X.; Yao, J.; Zhao, Y. S. Materials chemistry and engineering in metal halide perovskite lasers. Chem. Soc. Rev. 2020, 49, 951−982.
(131) Jia, Y.; Kerner, R. A.; Grede, A. J.; Rand, B. P.; Giebink, N. C. Factors that Limit Continuous-Wave Lasing in Hybrid Perovskite Semiconductors. Adv. Opt. Mater. 2020, 8, 1901514.
(132) Sutherland, B. R.; Hoogland, S.; Adachi, M. M.; Wong, C. T.; Sargent, E. H. Conformal Organohalide Perovskites Enable Lasing on Spherical Resonators. ACS Nano 2014, 8, 10947−10952.
(133) Wang, Y.; Li, X.; Song, J.; Xiao, L.; Zeng, H.; Sun, H. All-Inorganic Colloidal Perovskite Quantum Dots: A New Class of Lasing Materials with Favorable Characteristics. Adv. Mater. 2015, 27, 7101−7108.
(134) Zhao, J.; Yan, Y.; Wei, C.; Zhang, W.; Gao, Z.; Zhao, Y. S. Switchable Single-Mode Perovskite Microlasers Modulated by Responsive Organic Microdisks. Nano Lett. 2018, 18, 1241−1245.
(135) Cegielski, P. J.; Neutzner, S.; Porschatis, C.; Lerch, H.; Bolten, J.; Suckow, S.; Kandada, A. R. S.; Chmielak, B.; Petrozza, A.; Wahlbrink, T.; Giesecke, A. L. Integrated perovskite lasers on a silicon nitride waveguide platform by cost-effective high throughput fabrication. Opt. Express 2017, 25, 13199−13206.
(136) Duan, Z.; Wang, Y.; Li, G.; Wang, S.; Yi, N.; Liu, S.; Xiao, S.; Song, Q. Chip-Scale Fabrication of Uniform Lead Halide Perovskites Microlaser Array and Photodetector Array. Laser Photonics Rev. 2018, 12, 1700234.
(137) Cegielski, P. J.; Giesecke, A. L.; Neutzner, S.; Porschatis, C.; Gandini, M.; Schall, D.; Perini, C. A. R.; Bolten, J.; Suckow, S.; Kataria, S.; Chmielak, B.; Wahlbrink, T.; Petrozza, A.; Lemme, M. C. Monolithically Integrated Perovskite Semiconductor Lasers on Silicon

https://dx.doi.org/10.1021/acsphotonics.0c01394
ACS Photonics 2021, 8, 386−404

Photonic Chips by Scalable Top-Down Fabrication. Nano Lett. 2018, 18, 6915−6923.
(138) Du, W.; Zhang, S.; Shi, J.; Chen, J.; Wu, Z.; Mi, Y.; Liu, Z.; Li, Y.; Sui, X.; Wang, R.; Qiu, X.; Wu, T.; Xiao, Y.; Zhang, Q.; Liu, X. Strong Exciton−Photon Coupling and Lasing Behavior in All-Inorganic $CsPbBr_3$ Micro/Nanowire Fabry-Perot Cavity. ACS Photonics 2018, 5, 2051−2059.
(139) Yan, F.; Tan, S. T.; Li, X.; Demir, H. V. Light Generation in Lead Halide Perovskite Nanocrystals: LEDs, Color Converters, Lasers, and Other Applications. Small 2019, 15, 1902079.
(140) Shang, Q.; Zhang, S.; Liu, Z.; Chen, J.; Yang, P.; Li, C.; Li, W.; Zhang, Y.; Xiong, Q.; Liu, X.; Zhang, Q. Surface Plasmon Enhanced Strong Exciton-Photon Coupling in Hybrid Inorganic-Organic Perovskite Nanowires. Nano Lett. 2018, 18, 3335−3343.
(141) Su, R.; Diederichs, C.; Wang, J.; Liew, T. C. H.; Zhao, J.; Liu, S.; Xu, W.; Chen, Z.; Xiong, Q. Room-Temperature Polariton Lasing in All-Inorganic Perovskite Nanoplatelets. Nano Lett. 2017, 17, 3982−3988.
(142) Zhang, Q.; Su, R.; Liu, X.; Xing, J.; Sum, T. C.; Xiong, Q. High-Quality Whispering-Gallery-Mode Lasing from Cesium Lead Halide Perovskite Nanoplatelets. Adv. Funct. Mater. 2016, 26, 6238−6245.
(143) Tian, C.; Tong guo, T. g.; Zhao, S.; Zhai, W.; Ge, C.; Ran, G. Low-threshold room-temperature continuous-wave optical lasing of single-crystalline perovskite in a distributed reflector microcavity. RSC Adv. 2019, 9, 35984−35989.
(144) Evans, T. J. S.; Schlaus, A.; Fu, Y.; Zhong, X.; Atallah, T. L.; Spencer, M. S.; Brus, L. E.; Jin, S.; Zhu, X. Y. Continuous-Wave Lasing in Cesium Lead Bromide Perovskite Nanowires. Adv. Opt. Mater. 2018, 6, 1700982.
(145) Wang, X.; Shoaib, M.; Wang, X.; Zhang, X.; He, M.; Luo, Z.; Zheng, W.; Li, H.; Yang, T.; Zhu, X.; Ma, L.; Pan, A. High-Quality In-Plane Aligned $CsPbX_3$ Perovskite Nanowire Lasers with Composition-Dependent Strong Exciton-Photon Coupling. ACS Nano 2018, 12, 6170−6178.
(146) Gunnarsson, W. B.; Rand, B. P. Electrically driven lasing in metal halide perovskites: Challenges and outlook. APL Mater. 2020, 8, 030902.
(147) Kim, H.; Zhao, L.; Price, J. S.; Grede, A. J.; Roh, K.; Brigeman, A. N.; Lopez, M.; Rand, B. P.; Giebink, N. C. Hybrid Perovskite Light Emitting Diodes under Intense Electrical Excitation. Nat. Commun. 2018, 9, 4893.
(148) Zhao, L.; Roh, K.; Kacmoli, S.; Al Kurdi, K.; Jhulki, S.; Barlow, S.; Marder, S. R.; Gmachl, C.; Rand, B. P. Thermal Management Enables Bright and Stable Perovskite Light-Emitting Diodes. Adv. Mater. 2020, 32, 2000752.
(149) Qian, X.; Gu, X.; Yang, R. Lattice thermal conductivity of organic-inorganic hybrid perovskite $CH_3NH_3PbI_3$. Appl. Phys. Lett. 2016, 108, 063902.
(150) Xu, H.; Wang, X.; Li, Y.; Cai, L.; Tan, Y.; Zhang, G.; Wang, Y.; Li, R.; Liang, D.; Song, T.; Sun, B. Prominent Heat Dissipation in Perovskite Light-Emitting Diodes with Reduced Efficiency Droop for Silicon-Based Display. J. Phys. Chem. Lett. 2020, 11, 3689−3698.
(151) Xu, M.; Peng, Q.; Zou, W.; Gu, L.; Xu, L.; Cheng, L.; He, Y.; Yang, M.; Wang, N.; Huang, W.; Wang, J. A Transient-Electro-luminescence Study on Perovskite Light-Emitting Diodes. Appl. Phys. Lett. 2019, 115, 041102.
(152) Sytnyk, M.; Deumel, S.; Tedde, S. F.; Matt, G. J.; Heiss, W. A perspective on the bright future of metal halide perovskites for X-ray detection. Appl. Phys. Lett. 2019, 115, 190501.
(153) Kim, Y. C.; Kim, K. H.; Son, D. Y.; Jeong, D. N.; Seo, J. Y.; Choi, Y. S.; Han, I. T.; Lee, S. Y.; Park, N. G. Printable organometallic perovskite enables large-area, low-dose X-ray imaging. Nature 2017, 550, 87−91.
(154) Su, Y.; Ma, W.; Yang, Y. Perovskite semiconductors for direct X-ray detection and imaging. J. Semicond. 2020, 41, 051204.
(155) Mykhaylyk, V. B.; Kraus, H.; Saliba, M. Bright and fast scintillation of organolead perovskite MAPbBr3 at low temperatures. Mater. Horiz. 2019, 6, 1740−1747.
(156) Birowosuto, M. D.; Cortecchia, D.; Drozdowski, W.; Brylew, K.; Lachmanski, W.; Bruno, A.; Soci, C. X-ray Scintillation in Lead Halide Perovskite Crystals. Sci. Rep. 2016, 6, 37254.
(157) Ma, D.; Fu, Y.; Dang, L.; Zhai, J.; Guzei, I. A.; Jin, S. Single-Crystal Microplates of Two-Dimensional Organic−Inorganic Lead Halide Layered Perovskites for Optoelectronics. Nano Res. 2017, 10, 2117−2129.
(158) Kawano, N.; Koshimizu, M.; Okada, G.; Fujimoto, Y.; Kawaguchi, N.; Yanagida, T.; Asai, K. Scintillating Organic-Inorganic Layered Perovskite-type Compounds and the Gamma-ray Detection Capabilities. Sci. Rep. 2017, 7, 14754.
(159) Chen, Q.; Wu, J.; Ou, X.; Huang, B.; Almutlaq, J.; Zhumekenov, A. A.; Guan, X.; Han, S.; Liang, L.; Yi, Z.; Li, J.; Xie, X.; Wang, Y.; Li, Y.; Fan, D.; Teh, D. B. L.; All, A. H.; Mohammed, O. F.; Bakr, O. M.; Wu, T.; Bettinelli, M.; Yang, H.; Huang, W.; Liu, X. All-Inorganic Perovskite Nanocrystal Scintillators. Nature 2018, 561, 88−93.
(160) Maddalena, F.; Tjahjana, L.; Xie, A.; Arramel; Zeng, S.; Wang, H.; Coquet, P.; Drozdowski, W.; Dujardin, C.; Dang, C.; Birowosuto, M. Inorganic, Organic, and Perovskite Halides with Nanotechnology for High-Light Yield X- and γ-ray Scintillators. Crystals 2019, 9, 88.
(161) Heo, J. H.; Shin, D. H.; Park, J. K.; Kim, D. H.; Lee, S. J.; Im, S. H. High-Performance Next-Generation Perovskite Nanocrystal Scintillator for Nondestructive X-Ray Imaging. Adv. Mater. 2018, 30, 1801743.
(162) Nikl, M. Scintillation detectors for x-rays. Meas. Sci. Technol. 2006, 17, R37−R54.
(163) Pan, G.; Bai, X.; Yang, D.; Chen, X.; Jing, P.; Qu, S.; Zhang, L.; Zhou, D.; Zhu, J.; Xu, W.; Dong, B.; Song, H. Doping Lanthanide into Perovskite Nanocrystals: Highly Improved and Expanded Optical Properties. Nano Lett. 2017, 17, 8005−8011.
(164) Zhou, D.; Liu, D.; Pan, G.; Chen, X.; Li, D.; Xu, W.; Bai, X.; Song, H. Cerium and Ytterbium Codoped Halide Perovskite Quantum Dots: A Novel and Efficient Downconverter for Improving the Performance of Silicon Solar Cells. Adv. Mater. 2017, 29, 1704149.
(165) Kroupa, D. M.; Roh, J. Y.; Milstein, T. J.; Creutz, S. E.; Gamelin, D. R. Quantum-Cutting Ytterbium-Doped $CsPb(Cl_{1-x}Br_x)_3$ Perovskite Thin Films with Photoluminescence Quantum Yields over 190%. ACS Energy Lett. 2018, 3, 2390−2395.
(166) Sanchez-Carnerero, E. M.; Agarrabeitia, A. R.; Moreno, F.; Maroto, B. L.; Muller, G.; Ortiz, M. J.; de la Moya, S. Circularly polarized luminescence from simple organic molecules. Chem. - Eur. J. 2015, 21, 13488.
(167) Riehl, J. P.; Richardson, F. S. Circularly polarized luminescence spectroscopy. Chem. Rev. 1986, 86, 1−16.
(168) Longhi, G.; Castiglioni, E.; Koshoubu, J.; Mazzeo, G.; Abbate, S. Circularly Polarized Luminescence: A Review of Experimental and Theoretical Aspects. Chirality 2016, 28, 696−707.
(169) Zhang, C.; Sun, D.; Yu, Z.-G.; Sheng, C.-X.; McGill, S.; Semenov, D.; Vardeny, Z. V. Field-induced spin splitting and anomalous photoluminescence circular polarization in $CH_3NH_3PbI_3$ films at high magnetic field. Phys. Rev. B: Condens. Matter Mater. Phys. 2018, 97, 134412.
(170) Wang, J.; Zhang, C.; Liu, H.; McLaughlin, R.; Zhai, Y.; Vardeny, S. R.; Liu, X.; McGill, S.; Semenov, D.; Guo, H.; Tsuchikawa, R.; Deshpande, V. V.; Sun, D.; Vardeny, Z. V. Spin-optoelectronic devices based on hybrid organic-inorganic trihalide perovskites. Nat. Commun. 2019, 10, 129.
(171) Zhou, M.; Sarmiento, J. S.; Fei, C.; Zhang, X.; Wang, H. Effect of Composition on the Spin Relaxation of Lead Halide Perovskites. J. Phys. Chem. Lett. 2020, 11, 1502−1507.
(172) Chen, X.; Lu, H.; Li, Z.; Zhai, Y.; Ndione, P. F.; Berry, J. J.; Zhu, K.; Yang, Y.; Beard, M. C. Impact of layer thickness on the charge carrier and spin coherence lifetime in two-dimensional layered perovskite single crystals. ACS Energy Lett. 2018, 3, 2273−2279.
(173) Pan, X.; Liu, H.; Huynh, U.; Vardeny, Z. V. Magneto-electroluminescence response in 2D and 3D hybrid organic−

https://dx.doi.org/10.1021/acsphotonics.0c01394
ACS Photonics 2021, 8, 386−404

inorganic perovskite light emitting diodes. J. Chem. Phys. 2020, 152, 044714.
(174) Dang, Y.; Liu, X.; Sun, Y.; Song, J.; Hu, W.; Tao, X. Bulk Chiral Halide Perovskite Single Crystals for Active Circular Dichroism and Circularly Polarized Luminescence. J. Phys. Chem. Lett. 2020, 11, 1689−1696.
(175) Ma, J.; Fang, C.; Chen, C.; Jin, L.; Wang, J.; Wang, S.; Tang, J.; Li, D. Chiral 2D Perovskites with a High Degree of Circularly Polarized Photoluminescence. ACS Nano 2019, 13, 3659−3665.
(176) Shi, Y.; Duan, P.; Huo, S.; Li, Y.; Liu, M. Endowing Perovskite Nanocrystals with Circularly Polarized Luminescence. Adv. Mater. 2018, 30, 1705011.
(177) Chen, W.; Zhang, S.; Zhou, M.; Zhao, T.; Qin, X.; Liu, X.; Liu, M.; Duan, P. Two-Photon Absorption-Based Upconverted Circularly Polarized Luminescence Generated in Chiral Perovskite Nanocrystals. J. Phys. Chem. Lett. 2019, 10, 3290−3295.
(178) Kim, Y. H.; Zhai, Y.; Gaulding, E. A.; Habisreutinger, S. N.; Moot, T.; Rosales, B. A.; Lu, H.; Hazarika, A.; Brunecky, R.; Wheeler, L. M.; Berry, J. J.; Beard, M. C.; Luther, J. M. Strategies to Achieve High Circularly Polarized Luminescence from Colloidal Organic-Inorganic Hybrid Perovskite Nanocrystals. ACS Nano 2020, 14, 8816−8825.
(179) Szuromi, P. Polarized perovskite luminescence. Science 2020, 369, 640−641.
(180) Li, X.; Zhang, F.; He, H.; Berry, J. J.; Zhu, K.; Xu, T. On-device lead sequestration for perovskite solar cells. Nature 2020, 578, 555−558.
(181) Liang, H.; Yuan, F.; Johnston, A.; Gao, C.; Choubisa, H.; Gao, Y.; Wang, Y. K.; Sagar, L. K.; Sun, B.; Li, P.; Bappi, G.; Chen, B.; Li, J.; Wang, Y.; Dong, Y.; Ma, D.; Gao, Y.; Liu, Y.; Yuan, M.; Saidaminov, M. I.; Hoogland, S.; Lu, Z. H.; Sargent, E. H. High Color Purity Lead-Free Perovskite Light-Emitting Diodes via Sn Stabilization. Adv. Sci. 2020, 7, 1903213.
(182) Zou, C.; Chang, C.; Sun, D.; Bohringer, K. F.; Lin, L. Y. Photolithographic Patterning of Perovskite Thin Films for Multicolor Display Applications. Nano Lett. 2020, 20, 3710−3717.
(183) Zhang, L.; Yuan, F.; Xi, J.; Jiao, B.; Dong, H.; Li, J.; Wu, Z. Suppressing Ion Migration Enables Stable Perovskite Light-Emitting Diodes with All-Inorganic Strategy. Adv. Funct. Mater. 2020, 30, 2001834.

https://dx.doi.org/10.1021/acsphotonics.0c01394
ACS Photonics 2021, 8, 386−404